

https://dspace.org/

Effects of prenatal alcohol exposure on 3-week-old Sprague-Dawley rat proximal tibia: an immunohistochemical and three-dimensional micro computed tomography X-Ray investigation

Perry, Vaughan

2018
https://hdl.handle.net/10539/25252

Downloaded from a DSpace repository. https://dspace.org/

Effects of prenatal alcohol exposure on 3-week-old *Sprague-Dawley* rat proximal tibia: An immunohistochemical and three-dimensional micro computed tomography X-Ray investigation



Vaughan Perry

A Dissertation submitted to the Faculty of Health Sciences, University of the Witwatersrand, Johannesburg, in fulfilment of the requirements for the degree of Master of Science in Medicine

FACULTY OF HEALTH SCIENCES
UNIVERSITY OF THE WITWATERSRAND, JOHANNESBURG
2018

DECLARATION

I, Vaughan Perry, declare that this dissertation entitled “Effects of prenatal alcohol exposure on 3-week-old Sprague-Dawley rat proximal tibia: An immunohistochemical and three-dimensional micro computed tomography X-Ray investigation” is my own unaided work. It is being submitted for the Degree of Master of Science in Medicine at the University of the Witwatersrand, Johannesburg. It has not been submitted before for any degree or examination at any other University.



_____

Vaughan Perry

7 February 2018 at Parktown, Johannesburg.

ABSTRACT

Intrauterine alcohol exposure is detrimental to fetal and postnatal development. Fetal Alcohol Syndrome (FAS) is the most severe effect of prenatal alcohol exposure. Of the abnormalities that are characteristic of FAS, there are relatively few research studies on the effects of gestational alcohol exposure on skeletal development. Hence, we aimed at investigating the effects of prenatal alcohol consumption on the proximal growth plate of the tibia in 3 week old rats.

Time mated pregnant Sprague Dawley dams were assigned into either the ethanol (n=6), saline (n=6) control and untreated control groups (n=3). These rat dams were treated with 0.015 ml/kg of 25.2% ethanol and 0.9% saline by oral gavage during the 19 days of gestation respectively. While the untreated control group remained untreated. Two pups from each dame were selected from the three groups (n=60) and reared for three weeks. These pups were then terminated by intraperitoneal anesthetic injection of sodium pentobarbital. Following an abdominal incision the carcasses were fixed in 10% buffered formalin prior to the dissection of limbs.

Bilateral tibiae were harvested, soft tissue was cleaned off the tibiae and then these fixed in 10% buffered formalin. The proximal end of the left tibiae, was subjected to histological and immunohistochemical staining analysis. The, epiphyseal plate area, proliferative zone and hypertrophic zone length, number of cells, area, and number of proliferative cells where evaluated. For osteometric analysis bilateral tibiae were subjected to three-dimensional micro-focus computed tomography investigations.

The growth plate exhibited a smaller surface area as well as smaller proliferative and hypertrophic zones in the ethanol group. However the full and shaft length of the tibia was similar among all three groups. The total bone volume (BV/TV) and trabecular thickness (TbTh) were lower in the ethanol groups while trabecular number (TbN) was not affected in our study. There was a positive correlation between medullary canal area and cortical thickness. However, there was a negative correlation of BV/TV with trabecular number and spacing in the ethanol group.

Gestational alcohol exposure had an adverse effect on the growth plate with respect to its general size, respective zone sizes and the number of cells in each zone. This may be how diminished stature of the offspring occurs. Fewer proliferative cells were found using the anti-Ki67 antibody, indicating that in utero alcohol exposure slows cell proliferation, contributing to the small stature.

Logistic regression showed that the proximal medullary canal area and trabecular separation were the parameters affected the most in gestational alcohol exposure. The negative correlation of trabecular thickness and spacing in the ethanol group may contribute to bone weakness. These findings add knew knowledge to how in utero alcohol affects the offspring.

DEDICATION

To the women who made and molded me into the man I am today; Violet Irene Perry (1967-2010), Jane Jeanette Paulsen (1937-2008), Bernita Paulsen (1963-2016) and Valentine Lorraine Perry (1965-2010).

ACKNOWLEDGEMENTS

I would like to thank my funders NRF Thuthuka fund and JJJ Smieszieck grant. I am thankful to Mrs. Hasiena Ali for her training in histological and immunohistological staining procedures. I would like to humbly thank Mr. Kuda Jakata for his assistance in micro focus X-ray computed tomography scanning. Additionally, I would like to thank the staff of the Central Animal Services at the University of the Witwatersrand Medical School Parktown, for their assistance in the treatment of the study animals. Moreover I am thankful to the School of Anatomical Sciences University of the Witwatersrand for the consumables supplied throughout this project. I would like to further extend my deepest gratitude to Mrs. Diana Pillay for her unwavering guidance and support and Dr. Robert Ndou for his backing when it was most needed, his mentorship, empathy and candid guidance throughout this journey shaping me into a better individual. A great deal of thanks is due to Professor Amadi Ihwuno for the valuable advice he provided whenever it was needed. I am grateful to my family, in particular my grandmother Esther Perry and my aunt Maureen Perry for their support. To my brothers Khotso Bakwa, James Mchenga, Paballo Lephatsoe and friends, Tinashe Dube, Tihlelihle Magagula, Wandile Sishi, Mohlominyana Mofokeng and Ayotunde Awosusi, I would also like to extend my gratitude for the continual encouragement. To my fellow postgraduate students Shayla Pillay, Krytania Pather, and Nura Bello I would like to extend my appreciation for the support they gave when it was most needed.

TABLE OF CONTENTS

Declaration II

Abstract III

Dedication V

Acknowledgements VI

Table of Contents VII

List of abbreviations XI

List of figures XIV

Chapter 1: INTRODUCTION 1

1.1 Background to the research question 1

1.2 LITERATURE REVIEW 3

1.2.1 History of alcohol use 3

1.2.2 Classification of the effects of prenatal alcohol exposure 3

Fetal Alcohol Spectrum Disorder (FASD) 3

Fetal Alcohol Syndrome 4

1.2.3 Global FAS prevalence 5

1.2.4 Prevalence of FAS in South Africa 6

1.2.5 Bone development 7

Intramembranous ossification 7

Endochondral ossification 8

1.2.6 Appositional bone growth 10

1.2.7 Longitudinal bone growth and the epiphyseal plate 10

Resting Zone 11

Proliferative Zone 11

Hypertrophic Zone 11

Vascular Invasion Zone 11

1.2.8 Morphology of long bone 12

1.2.9 Microarchitecture of bone 13

Cortical bone 14

Trabecular bone 14

1.2.10 Bone modelling and remodeling 16

1.2.11 Bone imaging modalities 17

1.2.12 Imaging modalities used for the evaluation of bone mineral density 18
Dual – energy X-ray (DXA) 18
Quantitative computed tomography QCT 18
1.2.13 Imaging modalities used for the evaluation of bone architecture 19
Radiography 19
Magnetic Resonance Imaging (MRI) 19
1.2.14 Cell division and the cell cycle 20
Interphase 21
Mitotic phase 21
1.2.15 Determination of cell proliferation 23
The mitotic activity index 23
Thymidine labeling index 23
Bromodeoxyuridine labelling (BrdU) 24
Nucleolar organizer regions (NORs) 24
Flow cytometry 24
Immunohistochemical methods 25
1.2.16 The effects of prenatal alcohol exposure on human bone health 25
1.2.17 Animal models used to study the effects of prenatal alcohol consumption on bone health 26
1.2.18 Alcohol metabolism 28
1.3 AIMS AND OBJECTIVES 29
1.3.1 Aim 29
1.3.2 Study Objectives 29
CHAPTER 2: MATERIALS AND METHODS 30
2.1 Study animals 30
2.2 Study design 30
Allocation and treatment of animals 30
Birth and termination of pups 32
Tissue harvesting 33
Blood ethanol concentration (BEC) analysis. 33
2.3 Bone decalcification 34
2.4 Test for end point decalcification 35
2.5 Bone length measurement 35

2.6 Tissue processing 35
2.7 Paraffin wax embedding 36
2.8 Sectioning 36
2.9 Staining of tissue sections 39
Haematoxylin and eosin staining 39
Ki-67 Immunohistochemistry (IHC) 40
2.10 Light microscopy and photomicrography 41
Cell count 42
Cellular area 43
Growth plate area 43
Cellular proliferation 44
2.11 Three-dimensional micro-focus x-ray computed tomography (3D-µCT) 44
Parts of the tibia studied 45
Bone morphometry 47
2.12 Statistics analysis 48
CHAPTER 3: RESULTS 49
3.1 Measurement reliability 49
3.2 Blood alcohol concentration 49
3.3 Food consumed and weight gained during the gestation period 49
3.4 Gestation duration and litter size 50
3.5 Pups weights and crown rump length at 3 weeks of age 52
3.6 Histomorphometry and immunohistochemistry for Ki-67 protein 54
Epiphyseal plate surface area 54
Proliferative zone 54
Hypertrophic zone 57
3.7 Osteometry 59
Trabecular parameters 60
Proximal cross-sectional area, cortical area (thickness) and medullary canal area 61
Midshaft cross-sectional area, cortical area (thickness) and medullary canal area 64
Relationship of cross sectional area with cortical thickness and medullary thickness 66
Relationship of osteometric and trabecular morphometric parameters. 67
Prediction of group membership using the cortical and medullary canal areas 71
Prediction of group membership using the trabecular morphometric parameters 72

Parameters accounting for the ethanol group 73
Parameters accounting for the saline control group 76
chapter 4: Discussion 80
4.1 Rat model of fetal alcohol syndrome 80
4.2 Prenatal alcohol exposure effects on proximal tibia growth plate 82
Growth plate size 82
Proliferative zone surface area and cell count 82
Hypertrophic zone surface area and cell count 83
4.3 Osteometric and bone internal morphology 84
Bone length 84
Trabecular bone 86
4.4 Parameters most affected by prenatal ethanol exposure 88
CHAPTER 5: CONCLUSIONS 89
5.1 Limitations 89
5.2 Recommendations 89
Appendices 91
Appendix 1: Reagents used 91
Appendix 2: Equipment 93
Appendix 3: Software packages 94
Appendix 4: Preparation of 10% neutral buffered formalin (10%NBF) 95
Appendix 5: Determination of blood ethanol concentration 96
Appendix 6: Tissue decalcification 97
Appendix 7: Decalcification end point 98
Appendix 8: Tissue Processing 99
Appendix 9: Paraffin embedding 100
Appendix 10: Silane coated slides 101
Appendix 11: Staining of tissue sections 102
Appendix 11.1: Mayer's Haematoxylin and eosin staining 102
Appendix 11.2: Scott's tap water solutions 103
Appendix 11.3: Immunohistochemistry 103
Appendix 12.1 Cell count 106
Appendix 12.2: Measurement of cortical thickness 107
REFERENCES 108

LIST OF ABBREVIATIONS

%:	Percent
^{o}C:	Degree Celsius
β:	Beta
µm:	micrometer
dl:	deciliter
kg:	kilogram
ml:	milliliter
mg:	milligram
mm:	millimeter
nm:	nanometer
oz:	ounce
µCT:	Microfocus x-ray computed tomography
AESC:	Animal Ethics Screening Committee
ANOVA:	Analysis of variance
AP:	Alkaline phosphatase
APES:	3-aminopropyltriexothysilane
ARBD:	Alcohol-related birth defects
ARND:	Alcohol related neurodevelopmental disorder
BDMP:	Birth Defects Monitoring Program
BAC:	Blood alcohol concentration
BMD:	Bone marrow density

BMU: Basic multicellular unit

BrdU: Bromodeoxyuridine

BV: Bone volume

BT/TV Bone to total volume

CAS: Central animal services

CDC: Center for Disease Control and Prevention

CDK Cyclin dependent kinase

CNS: Central nervous system

CRL: Crown rump length

DAB: 3-3’ di-amino benzidine

DNA: Deoxyribose nucleic acid

EDC: Ethanol-derived calories

EDTA: Ethylenedeamine tetraacetic acid

FAS: Fetal alcohol syndrome

FASD: Fetal alcohol spectrum disorder

FIG: Figure

H_2O_2: Hydrogen peroxide

H&E: Haematoxylin and eosin

Ica: Ionized calcium

IHC: Immunohistochemistry

IOM: Institute of Medicine

IUFD: Intrauterine fetal death

IUGR:	Intrauterine growth restriction
µl:	Micro liter
MRI:	Magnetic resonance imaging
nmol:	Nanomole
NIAAA:	National Institute on Alcohol Abuse and Alcoholism
OFC:	Occipitofrontal circumference
PBS:	Phosphate buffer solution
pDXA:	Peripheral dual-energy x-ray absorptiometry
PFAS:	Partial fetal alcohol syndrome
pH:	Potential of hydrogen
PQCT:	Peripheral quantitative computed tomography
PTH:	Parathyroid hormone
RPS:	Rural Pediatric Services
Sa:	Sample interpolated concentration
SD:	Standard deviation
SES:	Socioeconomic status
Sv:	The amount of sample in each well
TbN	Trabecular number
TbSp:	Trabecular separation
TbTh:	Trabecular thickness
TV:	Total volume

LIST OF FIGURES

Figure 1.1: A child displaying facial dysmorphology associated with FAS 5
Figure 1.2: Connective tissue undergoing intramembranous ossification 8
Figure 1.3: Schematic representation of the process of endochondral ossification 9
Figure 1.4: Long bone undergoing circumferential growth 10
Figure 1.5: H&E stain of histological arrangement of epiphyseal growth plate. 12
Figure 1.6: Tibia of 3 week old rat. 13
Figure 1.7: Electron micrograph photo of Harversian canal. 15
Figure 1.8: Schematic representation of bone microarchitecture 16
Figure 2.1: Conceptual study design. 32
Figure 2.2: process of oral gavage. 33
Figure 2.3: Trimming of wax blocks 38
Figure 2.4: Serial sectioning of tissue. 39
Figure 2.5: Photomicrograph of the growth plate showing the proliferative and hypertrophic zones 44
Figure 2.6: Three-dimensional reconstruction of the tibia showing the parts that were investigated. 47
Figure 3.1: Food consumption 51
Figure 3.2: Weight gain 52
Figure 3.3: Overall weight gain 52
Figure 3.4: Weight of the pups at 3 weeks of age 54
Figure 3.5: The crown rump length of the pups at 3 weeks of age 54
Figure 3.6: Histomorphometry and Ki-67 positive cells in the tibia proximal epiphyseal plate proliferative zone. 56
Figure 3.7: Histomorphometry and Ki-67 positive cells in the tibia proximal epiphyseal plate hypertrophic zone. 58
Figure: 3.8: Measurements and volume. 59

Figure 3.9: Trabecular morphometric parameters (a) bone volume to total volume (BV/TV), (b) trabecular thickness (TbTh), (c) trabecular number (TbN), (c) trabecular spacing (TbSp). 61
Figure 3.10: Proximal cross-sectional area 62
Figure 3.11: Proximal medullary canal area.....62
Figure 3.12: Proximal cortical area. 63
Figure 3.13: Midshaft cross-sectional area.....64
Figure 3.14: Midshaft medullary canal area 64
Figure 3.15: Midshaft cortical area 65
Figure 3.16: Graphical representation of how the variables clustered 75
Figure 3.17: Graphical representation of how the variables clustered in three-dimensional space....78

CHAPTER 1: INTRODUCTION

1.1 Background to the research question

Teratogenic effects of alcohol consumption during pregnancy result in various forms of alterations in the development of the offspring. Jones and Smith (1973) described a classification for the associated characteristics resulting from gestational alcohol exposure. The features resulting from prenatal alcohol exposure are classified as fetal alcohol spectrum disorders (FASD). Fetal alcohol syndrome (FAS) which is a subcategory of FASD is the worst. Central nervous system (CNS) defects, facial dysmorphia and diminished growth are the main characteristics of FAS (Sokol and Clarren, 1989). While the effects of gestational alcohol exposure on the CNS are well known, the effects of the skeletal system have not been extensively investigated. These effects on the skeleton include, short stature due to smaller bones, osteoporosis and increased fracture risk (Miralles-Flores and Delgado-Baeza, 1992). Which account for 0.83% of the burden of disease globally, and 1.73% to the burden of disease in Europe (Johnell and Kanis, 2006).

Ethical considerations limit the type of research possible in humans. For example, pregnant woman may not be asked to consume alcohol for research purposes. Also, it is impossible to provide controlled conditions such as time and amount of alcohol intake among human research participants. As a result, these confounding factors are a challenge for alcohol research in pregnant woman. Consequently, animal models are used.

No safe amount of alcohol consumption during pregnancy has been established (Chaudhuri, 2000; Chakkalakal et al., 2002; Mikosch, 2014) . This fact, coupled with the increasing rate of alcohol use among woman and the high rates of FAS prevalence in South Africa pose a societal and health burden (Control and Prevention, 2003). This makes it appropriate for robust research studies to be conducted in order to obtain a basis for future interventions aimed at mitigating these effects.

The current study employed histological, immunohistological and micro focus X-ray computed tomography (CT) to understand how prenatal alcohol exposure affects bone development in the *Sprague-Dawley* rat tibia. First, we studied the proximal tibial growth plate to evaluate the observation that prenatal alcohol consumption results in diminished stature of the offspring (Chakkalakal et al., 2002; Keiver and Weinberg, 2004; Ramadoss et al., 2006). This involved a histomorphometric analysis of chondrocytes number and growth plate area. We proposed that reduced cell proliferation could contribute to the smaller stature observed in prenatal alcohol consumption. We then tested the validity of this theory by immunolabelling proliferating chondrocytes in the epiphyseal growth plate with the anti-Ki-67 antibody. Osteometric dimensions of the tibia were included to gain an estimation of bone size. The proximal part of the tibia was studied to understand how weak bones and osteoporosis may occur (Chakkalakal, 2005). This involved the use of Micro Computed Tomography (μCT) to quantify trabecular, thickness, number, separation and estimation of bone volume.

1.2 LITERATURE REVIEW

1.2.1 History of alcohol use

Alcohol use has been a part of both ancient and modern societies, being closely associated with celebrations and ceremonies (Parry, 2005). The culture of alcohol use is also apparent in South Africa, which has a rich history dating back to when settlers first landed on its shores. Cape Town, South Africa ; nicknamed the “tavern of the seas” by sailors using it as a refreshment station became a place of drunkenness and gambling (Parry, 2005). This was propagated by trade with natives for labour and cattle in exchange for liquor (Parry, 2005). Therefore, it is not surprising that South Africa has one of the highest rates of alcohol use in the world (Schneider et al., 2007).

There are gender differences in alcohol consumption. with more men (41.5%) drinking than females (17.1%) (Peltzer et al., 2011). However, recent studies indicate that the number of female drinkers is increasing and may be comparable to that of males in the future (Wilsnack et al., 2009; White et al., 2015). The tendency of increased alcohol use in females may result in an increased risk of alcohol induced disorders such as FAS (Slade et al., 2016).

1.2.2 Classification of the effects of prenatal alcohol exposure

Fetal Alcohol Spectrum Disorder (FASD)

The effects of prenatal alcohol exposure are classified from one general grouping called Fetal Alcohol Spectrum Disorder (FASD) (Sokol et al., 2003; Ethen et al., 2009). This (FASD) is further sub-classified into more specific conditions as follows: Alcohol-Related

Neurodevelopmental Disorder (ARND), Alcohol-Related Birth Defects (ARBD), Partial Fetal Alcohol Syndrome (pFAS) and the first to be discovered and most severe of the sub-classifications, Fetal Alcohol Syndrome (FAS).

Alcohol-Related Neurodevelopmental Disorder (ARND) is characterized by evidence of gestational alcohol exposure and both structural and functional neurological defects (Hoyme et al., 2005). Alcohol-Related Births Defects (ARBD) incorporate defects associated to gestational alcohol consumption such as bone problems, weakened immune system and heart problems (Hoyme et al., 2005). Partial Fetal Alcohol Syndrome (pFAS) includes some but not all characteristics of full FAS.

Fetal Alcohol Syndrome

The term Fetal alcohol syndrome was first reported by Jones and Smith in 1973 as a description of the features associated with gestation alcohol exposure. The diagnostic criteria for FAS include at least one growth abnormality, diagnosed central nervous system abnormality, three visible, distinctive facial abnormalities. The features of the latter are short palpebral fissures, thin upper lip and smooth philtrum (Fig. 1.1) (Landgraf et al., 2013). The central nervous system abnormalities have been extensively investigated in gestational alcohol exposure with paucity of research on the skeletal system. Therefore, further studies in this area are important.



Figure 1.1: A child displaying facial dysmorphology associated with FAS. A short palpebral fissure, thin vermillion and smooth philtrum (A) and lip grading scale for North white American (B) (Memo et al., 2013).

1.2.3 Global FAS prevalence

The average global prevalence of FAS is 0.97 per 1000 births (Abel, 1995; May et al., 2007). Abel and Sokol (1991) estimated an FAS prevalence of 0.33-2.2 per 1000 births in the United States of America. In African American communities of lower socioeconomic status the FAS prevalence rate was 2.3 per 1000 births (May et al., 2007). Native Americans have a higher prevalence of FAS at 8.5 per 1000 births (Duimstra et al., 1993).

In European countries, an FAS prevalence rate of 2.3 per 1000 births is reported for France, and 2.5 per 1000 births for Sweden (Sampson et al., 1997b). In Italy, a prevalence of 3.7-7.4 per 1000 births has been reported (Sampson et al., 1997b; May et

al., 2006). Prevalence studies were also carried out in Australia, stratified into the Western and the Northern territories. These studies used data sets from the Birth Defect Registry and the Rural Paediatric Services. They reported an estimate of 0.02 per 1000 births for non-aboriginal children and 2.76 per 1000 births for aboriginal children in the Western territory. In the Northern territory they found 0.68 per 1000 births for non-Aboriginal children and between 1.87-4.7 per 1000 births for Aboriginal children (O'Leary, 2004).

1.2.4 Prevalence of FAS in South Africa

Three independent studies carried out in the Western Cape show high FAS prevalances. The first study conducted by May et al. (2000) reports a prevalence of 40.5-46.4 per 1000 births. The second in this region recorded a prevalence of 65-74 per 1000 births, a substantial increase to the statistics previously reported (Viljoen et al., 2005). The third study by May and colleagues (2007) report a prevalence of 68.0-89.2 per 1000 births. In the Northern Cape, a prevalence of 67.2 per 1000 births was reported in Upington and De Aar (Urban et al., 2008).

The Center of Disease Control and Prevention (CDC) found a prevalence of 19 per 1000 births in Johannesburg. Though this figure is significantly lower than other studies in the country, it is still higher compared to developed countries (Warren et al., 2001; Control and Prevention, 2003).

1.2.5 Bone development

Intramembranous ossification

Intramembranous ossification occurs from a connective tissue membrane of mesenchymal cells and collagen fibers (Marcus et al., 2009). Ossification starts with the vascularization of the connective tissue, and the division and aggregation of the mesenchymal stem cells (Fig. 1.2) (Percival and Richtsmeier, 2013). These cells then differentiate forming osteoblasts which secret bone matrix. Alkaline phosphate then catalysis the calcification of this matrix by calcium salts, this traps osteoblasts in calcified bone matrix. These osteoblasts then differentiate into osteocytes (Fig. 1.2) (Kierszenbaum and Tres, 2015).

Numerous ossification centers form within the membrane, and interconnect with the progression of the ossification (Kierszenbaum and Tres, 2015). Trabeculae are established in this fashion, resulting in the formation of spongy bone. Through remodeling the outer layers of the bone will be converted to cortical bone with an arranged lamella system (Kierszenbaum and Tres, 2015). Therefore, bones formed by intramembranous ossification have three distinct layers; an inner spongy bone layer covered externally by a cortical bone layer (Kierszenbaum and Tres, 2015).

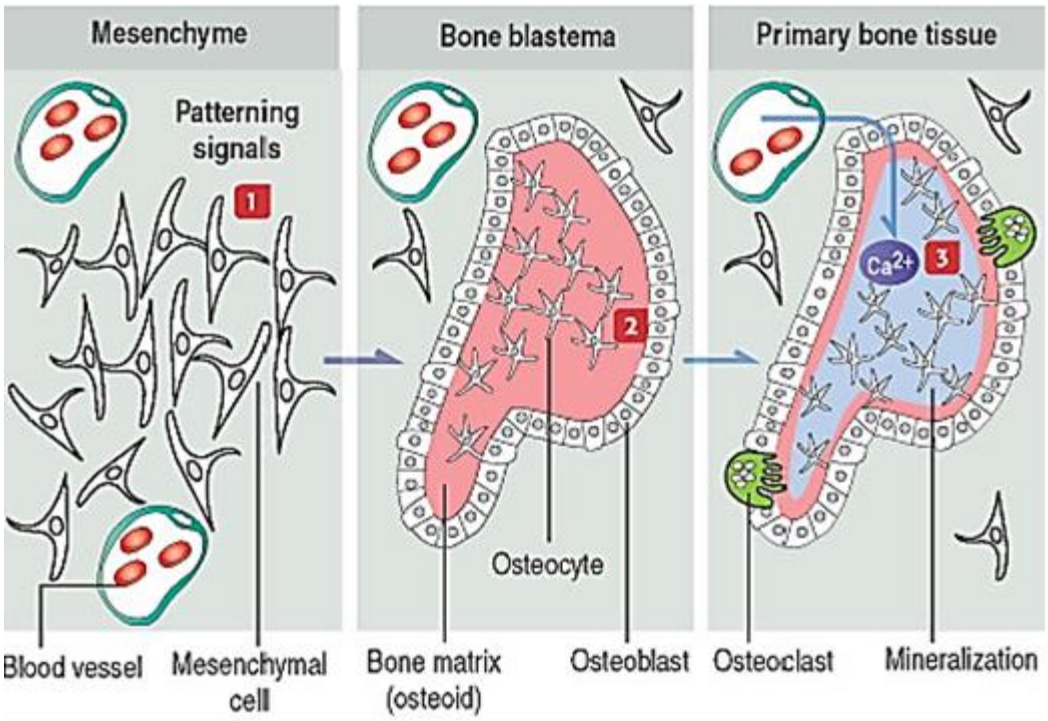

Figure 1.2: Connective tissue undergoing intramembranous ossification. The aggregation (1) and differentiation of mesenchymal stem cells into osteoblasts (2) which will finally lay down the bone matrix (3) (Kierszenbaum and Tres, 2015).

Endochondral ossification

Endochondral ossification (Fig. 1.3) occurs slower than intramembranous ossification, and involves the laying down of a cartilage precursor first (Kramer and Allan, 2005; White et al., 2011). The cartilage precursor becomes the model on which endochondral bone will be formed. As the hyaline cartilage model grows, chondrocytes in the midshaft start to enlarge as nutrient supply is limited. These enlarged chondrocytes begin to die leaving behind interconnecting spicules, which are there after calcified (Kramer and Allan, 2005; White et al., 2011). Simultaneously, a collar of bone is formed at the midshaft through intramembranous ossification. While vessels from the

periosteum penetrate the core of the diaphysis where there is a confluence of cavities caused by interconnecting spicules (Fig. 1.3). When the mesenchymal cells come in contact with the calcified matrix, they differentiate to form osteoblasts that lay down bone matrix. This will be the location of the primary ossification centre (Kramer and Allan, 2005; White et al., 2011). These vessels then further migrate to the ends of the cartilage model. The infiltration of the epiphyseal ends by blood vessels marks the formation of a secondary ossification centres (Kramer and Allan, 2005; White et al., 2011).

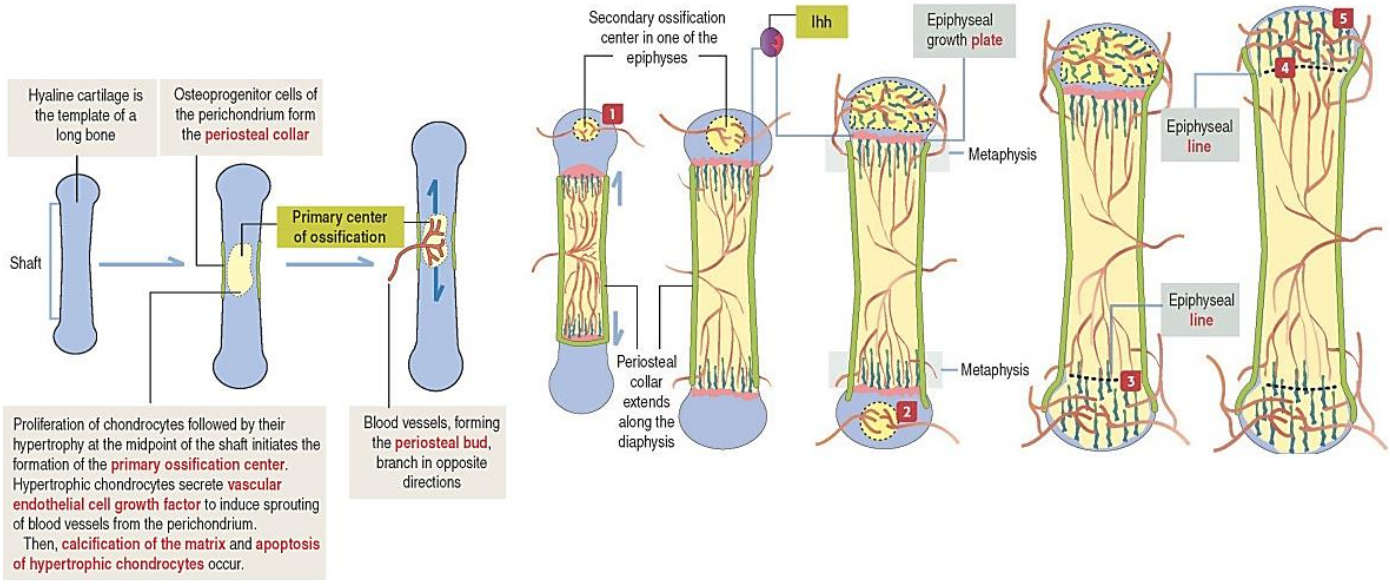

Figure 1.3: Schematic representation of the process of endochondral ossification. With the appearance of primary ossification centers in the diaphysis (1) , the appearance of secondary ossification centers in the proximally epiphysis (2), the replacement of the epiphyseal plate with the epiphyseal line (3), the intercommunication of the blood vessels from the diaphysis and the epiphysis (4) and finally the replacement of epiphyseal cartilage by bone (5) (Kierszenbaum and Tres, 2015).

1.2.6 Appositional bone growth

Osteoblasts in the periosteum deposit bone matrix on the external surface of bone. This matrix is calcified forming circumferential lamella (Kramer and Allan, 2005; White et al., 2011). Similarly, in the endosteum, osteoclast reabsorb bone matrix in the medullary cavity. This coupled action results in net growth in diameter of bone (Fig. 1.4) (Junqueira and Carneiro, 2005).

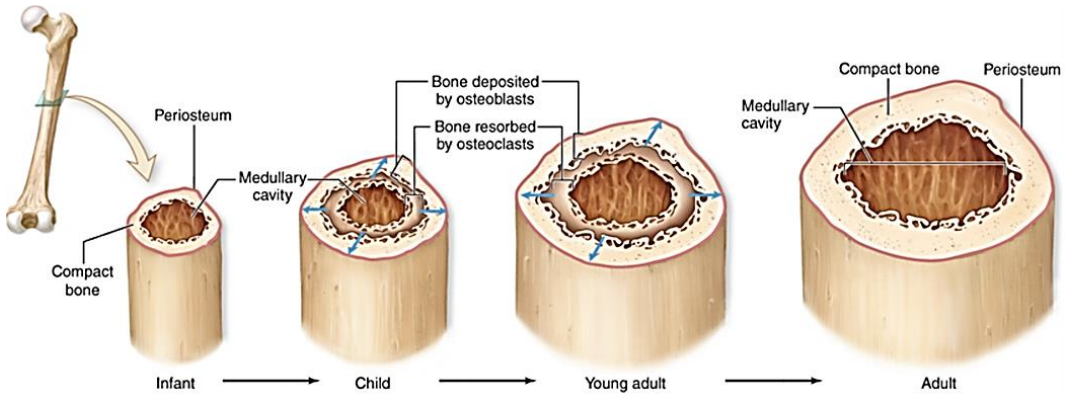

Figure 1.4: Long bone undergoing circumferential growth from infancy to adulthood. Bone is deposited in the periosteal layer while there is net bone reabsorption in the endosteal layer (Junqueira and Carneiro, 2005).

1.2.7 Longitudinal bone growth and the epiphyseal plate

The epiphyseal growth plate plays a central role in the longitudinal growth of long bones. It is located between the epiphysis and metaphysis, chondrocytes in this region are arranged in zones as show in figure 1.5. These zones from the epiphyseal end towards the metaphyseal end are; the resting zone, proliferative zone, hypertrophic zone and the vascular invasion zone (Kierszenbaum and Tres, 2015).

Resting Zone

Closest to the end of the epiphysis is the resting zone, in this zone chondrocytes are inactive. There is a large amount of extracellular matrix, in relation to the chondrocytes (Kierszenbaum and Tres, 2015).

Proliferative Zone

The second zone in the direction of the diaphysis is the proliferative zone; cells in this zone are in constant division resulting in longer, flattened rows of chondrocytes (Kramer and Allan, 2005; White et al., 2011). This zone is important in longitudinal growth.

Hypertrophic Zone

Within hypertrophic zone cells increases in size, then undergoes apoptosis, and calcification ensues (Kierszenbaum and Tres, 2015).

Vascular Invasion Zone

Hypertrophic cells attract blood vessels; these begin invading the calcified matrix. Blood vessels carry proteoblasts into this region, these differentiate into osteoblasts which will secret osteoid (Kramer and Allan, 2005; Kierszenbaum and Tres, 2015).

Progression of the medullary cavity into the hypertrophic zone produces longitudinal growth of the diaphysis. This invasion is countered by the rapid division of chondrocytes in the proliferative zone, maintaining the length of the epiphyseal growth plate. This growth plate diminishes in length with age until its closure when the

metaphysis comes in contact with the epiphysis (Kramer and Allan, 2005; White et al., 2011). Any disruption to these zones such as the effects of gestational alcohol exposure result in stunted longitudinal growth in the bone.

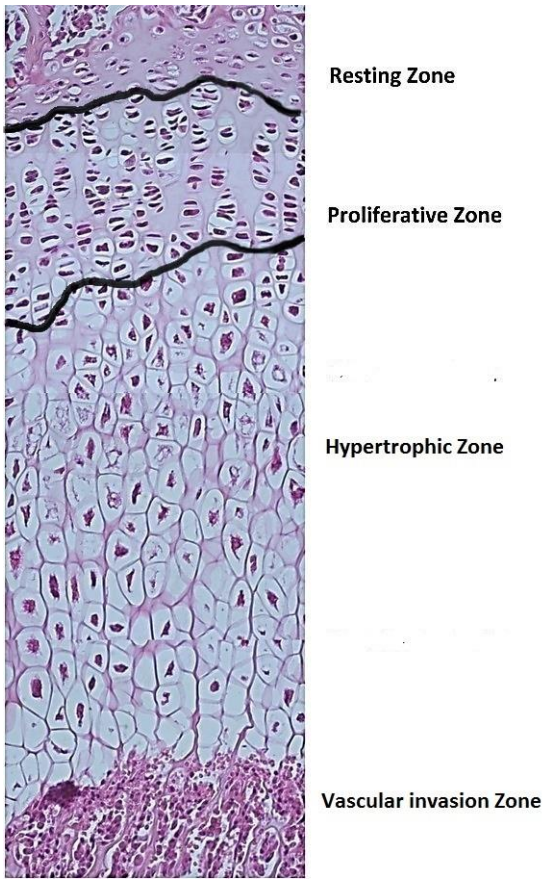

Figure 1.5: H&E stain of histological arrangement of epiphyseal growth plate. The sparsely arranged resting zone, followed by the column stacked proliferative zone with flattened chondrocytes and the enlarged chondrocytes in the hypertrophic zone. Closest to the metaphysis is the vascular invasion zone (Image, courtesy of PERRY. V).

1.2.8 Morphology of long bone

To investigate the effects of gestational alcohol exposure, an understanding of bone structure is essential. Bone supports soft tissue during locomotion, protects vital organs

and maintains mineral homeostasis (Kramer and Allan, 2005; White et al., 2011). Four bone types exist; long, short, flat, and irregular bones. Since *in-utero* alcohol exposure results in growth inhibition and considering that long bones are essential for height and growth, (Nwaogu, 2002; Simpson et al., 2005; Snow and Keiver, 2007), this study will pay attention to long bones. The morphology of long bones includes a cylindrical shaft called the diaphysis, and flared ends called a metaphysis and capped ends called the epiphysis (Fig. 1.6).

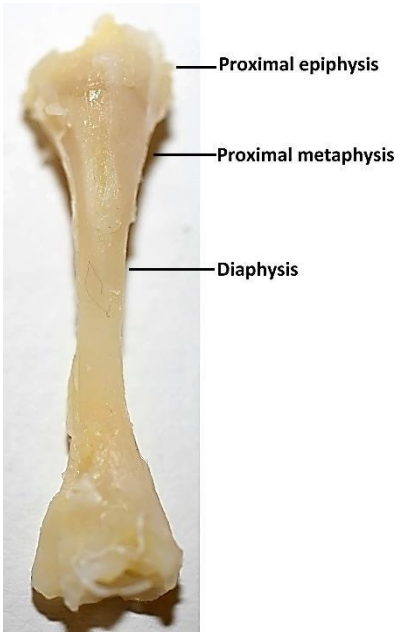

Figure 1.6: Tibia of 3 week old rat. The epiphysis, metaphysis and the diaphysis (Image, courtesy of R Ndou)

1.2.9 Microarchitecture of bone

Previous studies reported that alcohol causes a decrease in bone mass and alterations in trabecular and cortical bone (Hogan et al., 1997; Soares et al., 2010; Maurel D. B et al., 2012). This results in a decrease in mechanical strength and an increase in

osteoporosis as well as fracture risk. An understanding of the morphology and histology of cortical and trabecular bone is necessary to investigate the effects of gestational alcohol exposure on these components of bone. There are two categories of bone tissue based on histological porosity and microarchitecture. These are cortical and trabecular bone.

Cortical bone

Previous studies show that alcohol causes a decrease in compact bone thickness in young growing rats (Sampson et al., 1996). Cortical bone is mainly found in the diaphysis. It is composed of harversian systems which are made up of cylindrical subunits called interstitial lamella (Fig**.** 1.8) (Kramer and Allan, 2005; Marcus et al., 2009; White et al., 2011). Interstitial lamella surround canals called harversian canals. Within the lamella are small cavities containing osteocytes called lacunae (Fig. 1.7). The interstitial lamella is found between the outer circumferential lamella and the inner circumferential lamella which lies on the marrow surface of shaft (Kramer and Allan, 2005; Marcus et al., 2009; White et al., 2011). Volkmann's canals run perpendicular to the longitudinal axis of the diaphysis. Both the Haversian and Volkmans canals contain blood vessels, lymphatic's and nerves (Kramer and Allan, 2005; White et al., 2011).

Trabecular bone

Alcohol causes adverse effects on trabeculae. A study by Maurel D. B et al. (2012) reported that alcohol consumption resulted in thinner trabeculae in both the distal femur metaphysis and vertebral body. This corroborates earlier findings of decreased

trabecular thickness in the proximal tibia metaphysis of alcohol-fed rats (Reed et al., 2002). Since reduced thickness may decrease strength, it escalates fracture risk in alcohol exposed offspring (McCall et al., 2006).

Trabecular bone is found in axial skeletal elements, the metaphysis and epiphysis of long bones, it accounts for 20% of the adult human skeleton (Clarke, 2008). It consists of trabecular plates and rods, which connect to form cavities that have a lattice like appearance housing bone marrow (Fig. 1.8) (Kramer and Allan, 2005; White et al., 2011). This arrangement of trabecular bone makes it porous in nature. Bone marrow cavities are lined by one cell layer thick connective tissue called the endosteum. This layer contains osteoblasts and osteoclasts (Fig. 1.8) (Kramer and Allan, 2005; White et al., 2011).

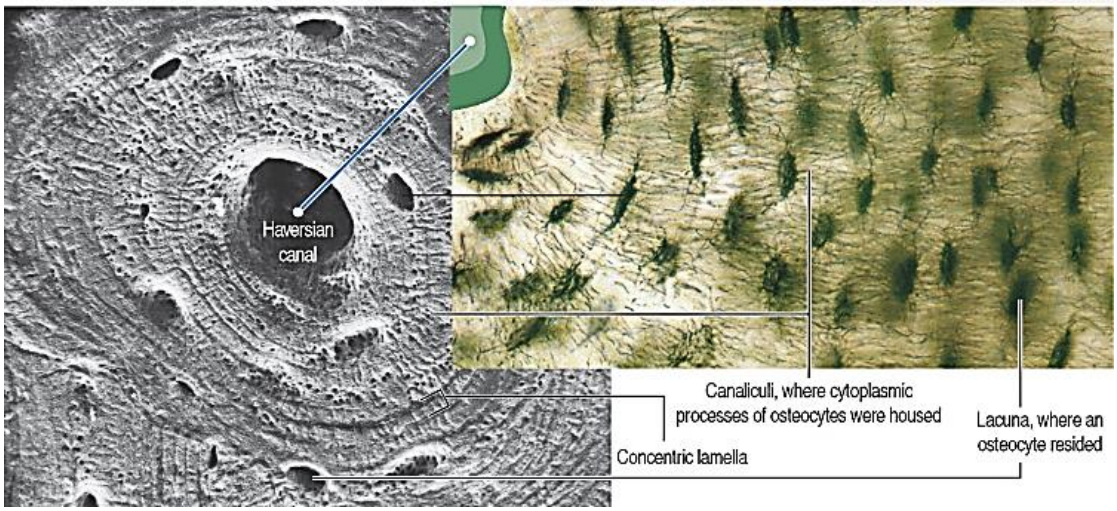

Figure 1.7: Electron micrograph of Harversian canal. Canal surrounded by concentric lamella, with lacuna embedded within. Canaliculi project from lacuna (Weiner et al., 1999) .

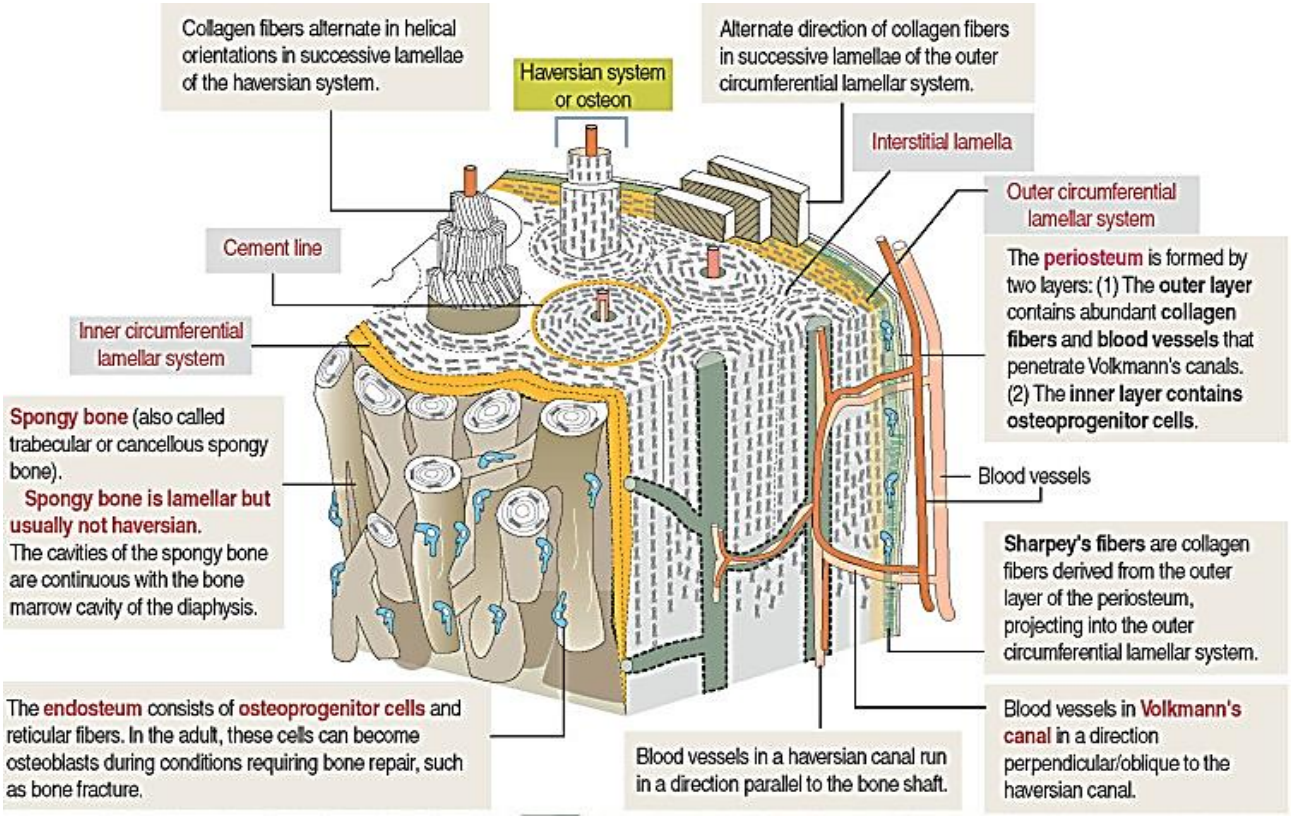

Figure 1.8: Schematic representation of bone microarchitecture (Kierszenbaum and Tres, 2015).

1.2.10 Bone modelling and remodeling

Bone remodeling is a process where bone is being renewed to maintain its functional abilities. Osteoblasts are responsible for the deposition of the bone matrix and facilitating the mineralization of the matrix. Osteoclasts are responsible for the reabsorption, and demineralization of the bone matrix (Ducy et al., 1996; Clarke, 2008). These are arranged in units known as bone multicellular units (BMU), which are arranged differently in cortical and trabecular bone (Hadjidakis and Androulakis, 2006).

The remodeling of bone happens in three phases; reabsorption, reversal and formation (Hadjidakis and Androulakis, 2006).

- Reabsorption Phase is characterized by the migration of partially differentiated mononucleated preosteoclast to the bone surface where they form multinucleated osteoclasts.
- Reversal Phase follows the reabsorption phase by migration of mononucleated cells to the bone surface. These produce signals for osteoblast differentiation.
- Formation phase follows with osteoblast laying new bone.

Similar to bone remodeling, bone modelling is facilitated by the reabsorption or the deposition of new bone. But as opposed to bone remodeling, bone modelling is not in response to damage but rather loading. The process of bone deposition and bone reabsorption happens at equilibrium, thus maintaining a set amount of bone density (Cooper et al., 2002). Should there be a net imbalance in the reabsorption and deposition of bone this would result in an increase or decrease in bone density and greatly affect bone health and strength.

1.2.11 Bone imaging modalities

Bone imaging modalities employ two general measures for bone health: bone mass and bone strength/quality (Grampp et al., 1999; Griffith and Genant, 2011). Bone mass is a measure of bone mineral density and is the standard in the evaluation of bone health.

Bone quality is observed through trabecular and cortical microarchitecture (Grampp et al., 1999). The imaging modalities used in the evaluation of bone health are set up to respond to either bone mineral density (BMD) or bone microarchitecture.

1.2.12 Imaging modalities used for the evaluation of bone mineral density

Dual – energy X-ray (DXA)

Dual – energy X-ray (DXA) is the gold standard used to evaluate bone mineral density (Grampp et al., 1999; D'Elia et al., 2009). This is done from a composite image created by two x-ray beams: one beam emitting low energy radiation the other relatively high energy radiation. From this information bone mineral density can be evaluated in a two dimensional plane (mg/cm^2) (Bauer and Link, 2009). This technique administers relatively low radiation when compared to other imaging modalities. This feature makes it advantageous in clinical settings. However, the disadvantage is that DXA provides a composite measure of mineral density for both cortical and trabecular bone (Griffith and Genant, 2011).

Quantitative computed tomography QCT

Quantitative computed tomography is derived from the recent computed tomography technology (Donnelly, 2011). This method employs a detector to capture electrons from an x-ray beam. These electrons are absorbed or pass through the specimen depending on its density (Kherlopian et al., 2008; Donnelly, 2011). This provides volumetric information (Household Units-HU) about the tissue (D'Elia et al., 2009; Griffith and Genant, 2011). Additionally in QCT a bone mineral phantom is introduced

in the imaging field, allowing the conversion of HU to bone mineral equivalents (mg/cm^3) (Grampp et al., 1999; D'Elia et al., 2009). As a result BMD information reported by QCT is volumetric, and information about cortical bone is discriminated from trabecular bone (D'Elia et al., 2009). Therefore, this technique is more sensitive than DXA but administers a greater radiation dose.

1.2.13 Imaging modalities used for the evaluation of bone architecture

Radiography

Radiography uses basic x-ray technology; an electromagnetic beam is directed towards a specimen with a detector to record the amount of absorption by the tissue on adjacent side (Link and Majumdar, 2004). This method provides a 2D representation of the tissue with high spatial resolution, but lacks consistency in visualizing the trabecular (Griffith and Genant, 2011).

Magnetic Resonance Imaging (MRI)

Magnetic Resonance Imaging (MRI) is unique amongst the imaging techniques in that it employs magnetic fields in the analysis of tissue instead of ionized radiation (Link and Majumdar, 2004). The magnetic field is directed to the hydrogen in the water content of tissue. Because bone has a low water content it is a poor respondent to the technique. Consequently, trabecular is visualized as dark spaces around the bright bone marrow which has relatively high water content (Link and Majumdar, 2004; Donnelly, 2011). This method is favorable in clinical setups as it does not expose the patient to ionizing radiation. However, the disadvantage is that this method requires a

long scanning time to achieve high spatial resolution of trabecular bone (Grampp et al., 1999).

Micro computed tomography (μCT)

Micro computed tomography employs the same concept of electromagnetic beams directed towards a specimen, except in this instance it is done in rotational manner. Resulting a three dimensional representation of the tissue, with high spatial resolution (up to 50 μm) after the geometric reconstruction of the specimen (Link and Majumdar, 2004; Bauer and Link, 2009). This allows the in-depth investigation of the tissue without their destruction. It is achieved by administering large doses of electromagnetic radiation, making this technique suitable for experimental in-vitro studies. Thus it was chosen as the more suitable technique for the present study.

1.2.14 Cell division and the cell cycle

Cell differentiation and specialization is preceded by a tightly controlled cell division process, which comprises of 6 stages namely: prophase, prometaphase, metaphase, anaphase, telophase and cytokinesis (Table. 1.1) (Young et al., 2013). The division of a cell producing two identical daughter cells is mitosis, a process that occurs within somatic cells (Reece et al., 2014). This cellular process results in two cells with a diploid number of chromosomes, which is 22 pairs of autosomes and 2 pairs of sex chromosomes (Reece et al., 2014). This process is then followed by cytokinesis which is the division of the cytoplasm. Mitosis and cytokinesis are but two steps in the cell cycle,

alternating with interphase which makes up about 90% of the cell cycle (Reece et al., 2014).

Interphase

Interphase is comprised of 3 phases; G_1 phase, S phase and G_2 phase. All three stages are concerned with cell growth and the production of cytoplasmic organelles. Chromosomes will duplicate during the S phase of interphase (Reece et al., 2014).

Mitotic phase

The mitotic stage is responsible for cell division; it is divided into five phases. These are prophase, prometaphasae, metaphase, anaphase and telophase; the latter is overlapped by cytokinesis. The milestones in each of these stages are summarized in table 1.1.

Table 1.1: The milestones of the different stages of the mitotic phase of the cell cycle.

	Centromeres	Chromatids	Nucleus	Cytoplasm	Chromosome
Prophase	Mitotic spindle forms. Centromeres move away from each other.	Form chromosomes.	Nucleoli disappears.	-	Chromatin fibers become tightly coiled.
Prometaphase	Microtubules attached to tubules from the opposite side.	Each chromatid has a kinetochore. Microtubules attach to the kinetochore.	Nuclear envelope fragments. Microtubules invade nuclear area.	-	Chromosomes are even more condensed.
Metaphase	Each centromere is now at the opposite end.	-	-	-	Chromosomes are arranged at metaphase plate.
Anaphase	-	Two sister chromatids part. Each chromatid becomes full chromosome.	-	-	Two sets of chromosomes formed. Chromosomes are pull to each end.
Telophase		-	Two nucleoli form in the cell. Nuclear envelop starts to form.		Become less condensed
Cytokinesis				Formation of a cleavage furrow and final division of cytoplasm.	

1.2.15 Determination of cell proliferation

Several techniques have been developed to detect the passage of cells through the cell cycle. They include; the mitotic activity index, thymidine labelling index, bromodeoxyuridine labelling, nucleolar organizer regions, flow cytometry and immunohistochemical methods (Brown and Gatter, 1990; Barnes and Gillett, 1995; Scholzen and Gerdes, 2000).

The mitotic activity index

The mitotic activity index makes up the most primitive technique employed in the quantification of cellular proliferation. It can be used on tissue normally fixed and stained with heamatoxylin and eosin (Brown and Gatter, 1990; Barnes and Gillett, 1995; Scholzen and Gerdes, 2000). It employs the analysis of mitotic figures per high power fields averaged from 10 consecutive fields. Although this method is cheap, mitosis might be confused for pyknotic nuclei (Brown and Gatter, 1990; Barnes and Gillett, 1995; Scholzen and Gerdes, 2000).

Thymidine labeling index

The thymidine labelling index method introduced in the 1950's, utilizes the uptake of tritiated thymidine in DNA synthesis (Brown and Gatter, 1990; Barnes and Gillett, 1995; Scholzen and Gerdes, 2000). This method proved to be slow and imprecise because the uptake is illustrated through auto-radiography (Brown and Gatter, 1990; Barnes and Gillett, 1995; Scholzen and Gerdes, 2000). Additionally, the methods required the use of fresh tissue.

Bromodeoxyuridine labelling (BrdU)

The introduction of bromodeoxyuridine (BrdU) labelling as an improvement to thymidine labelling techniques, came with advantages such as the ability to label samples in-vivo and in-vitro (Brown and Gatter, 1990). This technique incorporates BrdU which is taken-up during S phase (Brown and Gatter, 1990; Barnes and Gillett, 1995).

Nucleolar organizer regions (NORs)

Nucleolar organizer regions (NORs) are also employed as markers for proliferation as they reflect the production of ribosomal components, and protein production within the cell. Although this method can only analyze a small number of cells at a time (50-100), and considering the fact that NORs are hard to identify and are not consistent this method was regarded irrelevant (Brown and Gatter, 1990; Barnes and Gillett, 1995).

Flow cytometry

Flow cytometry has evolved from being used as a cell counting technique in 1960's, to the measurement of nuclear DNA and fluorescence labelled antibodies in the 1990 (Brown and Gatter, 1990). Although this technique can analyze a large number of cells in a short period of time, it results in the loss of morphology. Additionally the instrument is expensive (Brown and Gatter, 1990; Barnes and Gillett, 1995).

Immunohistochemical methods

With regards to immunohistochemical methods, the first technique used is the Ki-67 antibody, which recognizes the Ki-67 antigen associated with the cell nucleus (Brown and Gatter, 1990; Scholzen and Gerdes, 2000). The Ki-67 antigen is produced in all stages of the cell cycle except the quiescent or resting stage (G_0 phase). The amount of Ki-67 present in a cell reaches peak G_2 and M phase, though it is tightly associated to cell proliferation its fundamental role in the cell cycle is unknown (Brown and Gatter, 1990; Barnes and Gillett, 1995; Scholzen and Gerdes, 2000). This technique proved very relevant in that the Ki-67 could be identified in all types of cells, throughout different phases in the cell cycle (Brown and Gatter, 1990; Barnes and Gillett, 1995; Scholzen and Gerdes, 2000)

1.2.16 The effects of prenatal alcohol exposure on human bone health

Prenatal alcohol exposure has direct and indirect effects on bone growth and morphology, which may affect chondrocytes and osteoblasts (Simpson et al., 2005). Indirect effects on bone development include disruption of maternal and fetal physiology by altering the growth factor hormone or its inhibitor and activators. Smith et al. (1981) reported a decrease in mean bone age in children exposed to alcohol prenatally. Habbick et al. (1998) noted a decrease in bone mass. Furthermore, It is well established that offspring exposed to alcohol in-utero undergo minimal catch up growth in postnatal life, with effects persisting until the age of 14 (Streissguth et al., 1991; Day et al., 2002).

Presently studies on the effects of gestational alcohol consumption on postnatal development are limited in both animal and human studies. It is crucial to gain insight on the effects of prenatal alcohol exposure on postnatal development since it is suggested that osteoporosis and an increased risk of fractures may occur in adulthood (Cooper et al., 1997; Habbick et al., 1998; Simpson et al., 2005).

1.2.17 Animal models used to study the effects of prenatal alcohol consumption on bone health

The use of animal models to determine the effects of prenatal alcohol exposure ensures a controlled environment and better handling of external factors. Results of the epidemiological and pathological effects on animals are useful in supporting human related findings. Early animal models range from zebrafish (*Danio rerio),* guinea pigs and sheep and rodents (Patten et al., 2014). The choice of animal model is reliant on the aim of the experiment, the animal's genetic composition and mechanism of action of the experimental substance (Patten et al., 2014). It is also important to ensure that the animal model has similar growth patterns as humans.

Rodents, in particular the rat model has been extensively used in the research of the prenatal effects of alcohol on skeletal development. The rat model is advantageous because they have been greatly explored scientifically. Therefore, a great amount of literature on different scientific explorations with regards to the anatomy, physiology and behavior is available (Cudd, 2005). Further, rats have short gestation periods (21 days) and a relative large litter size.

Table 1.2: Summary of the physical effects of prenatal alcohol consumption

Author	Model	Development stage	Findings
Carvan et al. (2004)	Zebrafish		Craniofacial and neurocranial dysmorphogenesis.
Ramadoss et al. (2006)	Sheep	Postnatal	Decrease bone strength.
Chernoff (1977)	Mice	Prenatal	Deficient ossification.
Mishra et al. (2003)	Mice	Prenatal	Delayed ossification.
Mehta et al. (2002)	Rat	Postnatal	Decreased body weight. Decreased bone mineral content. Decreased bone mineral density.
Miralles-Flores and Delgado-Baeza (1992)	Rat	Prenatal/ Postnatal	Decreased tibia length. Decreased growth plate Decrease in number of cells (Proliferative zone) Decreased height (Hypertophic zone).
Simpson et al. (2005)	Rat	Prenatal	Decreased body weight. Decreased skeletal ossification.
Snow and Keiver (2007)	Rat	Prenatal	Decrease in tibia length. Disruption in histology of epiphysis.
Keiver et al. (1996)	Rat	Prenatal	Decrease body weight. Decrease in length. Decrease in ossification.

1.2.18 Alcohol metabolism

The principle enzymes responsible for the oxidation of alcohol are Alcohol dehydrogenase (ADH) and cytochrome P-450 (Cederbaum, 2012). These are predominantly found in the liver. Alcohol orally ingested will undergo first pass metabolism in the stomach, before it reaches the systemic circulation. This in undertaken by ADH isoform namely σADH, class I and III ADH (Cederbaum, 2012). Therefore this may result in lower alcohol concentrations.

Alcohol absorption is by passive diffusion down a concentration gradient, and therefore it is subject to tissue water content, tissue mass and rate of blood flow (Cederbaum, 2012). Thus the same alcohol dose will be differently distributed and further metabolised in individuals depending on factors such body weight and fat to water content (Cederbaum, 2012). Furthermore the metabolism of alcohol is correlated to basal metabolic rate; therefore animals with small body weights will metabolism alcohol faster than larger animals (Refinetti, 1989).

1.3 AIMS AND OBJECTIVES

1.3.1 Aim

This study sought to investigate the effects of intrauterine alcohol exposure on the postnatal bone development of the proximal rat tibia.

1.3.2 Study Objectives

1. To test whether gestational alcohol exposure affects the tibial growth plate, an histomorphometric analysis of area and chondrocytes number in the proliferative and hypertrophic zones, as well as growth plate area was conducted.
2. To investigate whether gestational alcohol exposure affects tibial growth plate cell proliferation, immunolabelling with Ki-67 antibody was conducted and dividing cells in the proliferative and hypertrophic zones quantified.
3. To investigate whether gestational alcohol exposure affects internal tibial bone morphology, a morphometric analysis of diaphyseal length, cortical thickness, as well as trabecular thickness, volume, spaces and number was done using 3D microfocus x-ray computed tomography.

CHAPTER 2: MATERIALS AND METHODS

2.1 Study animals

Fifteen (15), three-months-old, virgin female *Sprague-Dawley* rats weighing an average of 300g were used. All the animals were obtained and housed at the Central Animal Services (CAS), University of the Witwatersrand. The animals were housed in transparent plastic cages lined with wood dust, with unlimited access to food and water. Room temperature was maintained at 23±2°C and a 12-hour light-dark cycle. The study was approved by the Animal Ethics Screening Committee (AESC), University of the Witwatersrand, Johannesburg (AESC 2015/27/15C).

2.2 Study design

Allocation and treatment of animals

Animals were randomly allocated to three groups; ethanol group, saline controls and untreated controls (Fig. 2.1). The appearance of vaginal plug was considered day one of gestation; on this this day treatment was started. The ethanol group (n=6) received 0.015ml/kg body weight of 25.2% ethanol once daily for 19 days via oral gavage from the first day of gestation (Fig. 2.2). With respect to controls, the saline control group (n=6) received 0.015ml/kg body weight of 0.9% saline via the same route and for the same duration. The untreated control group (n=3) received neither alcohol nor saline.

Fewer animals were used in the latter group to reduce the number of animals used in the study.

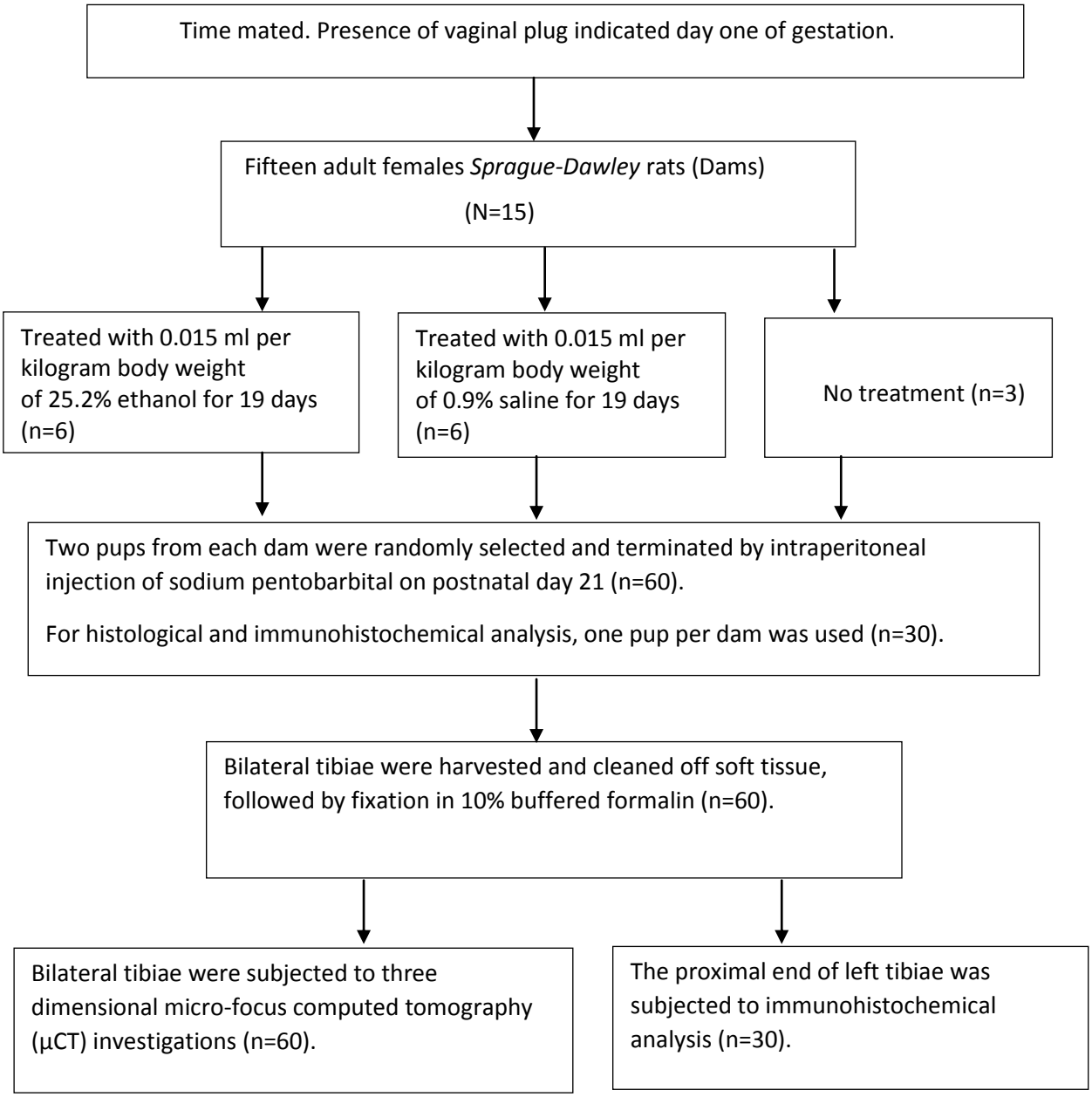

Figure 2.1: Conceptual study design

To monitor growth and general health, the dams were weighed daily at approximately 10h00 using an electronic weighing scale (Snowrex Electronic Scale, Clover Scales, Johannesburg). Food consumed daily was also measured, and considered to be the difference between the weight of the food remaining in the feeding trough and that of the food given the previous morning. To determine peak blood ethanol concentration,

tail vein blood samples were collected weekly, an hour after oral gavage (See section "Blood ethanol concentration (BEC) analysis").



Figure 2.2: Process of oral gavage. Animal was held gently by grasping the loose skin on the back and the neck. Gavage needle was passed along the side of the mouth into the esophagus and towards the stomach. The solution was then gently passed directly in to the stomach (Image courtesy of R. Ndou).

Birth and termination of pups

The birth day of the pups in each litter was designated as postnatal day zero. The litter size was recorded upon birth and the pups reared freely with their dams for 21 days. On postnatal day 21, two pups (n=30) from each of the dams (n=15) were randomly selected, weighed and crown rump length measured. The pups were then terminated by an intraperitoneal anesthetic injection of sodium pentobarbital. A thoraco-pelvic

midline abdominal incision was made and slits were made on the skin covering the limbs to allow penetration of the fixative. Then the entire carcass was immediately immersed in freshly prepared 10% buffered formalin (Appendix 1) prior to dissection of the limbs.

Tissue harvesting

Bilateral hind limbs were carefully dissected and detached from the acetabulum using a pair of scissors, forceps and scalpel blade which were also used to remove all non-bony tissues. Knee joints were disarticulated and tibiae were removed, cleaned and subsequently immersed in fresh 10% buffered formalin for 24 to 72 hours prior to Miro CT scanning (see section 2.8) and later tissue processing for histological analysis (see section.2.5).

Blood ethanol concentration (BEC) analysis.

Tail vein blood (100 to 200µl) was collected into heparinized capillary tubes (Modulohm Vitrex®). Each capillary tube was shut with prestick on both ends to retain the blood. Then paper towel was used to wrap the capillary tube before placing them individually into plastic bottles. These blood samples were immediately placed on ice. Within an hour after collection, all samples were then stored at -80°C for preservation until analysis.

Microcapillary tubes were thawed to room temperature and spun in a microhaematocrit centrifuge (Haematokrit 210, Hettich, Germany) at 3000 rpm for 10 minutes. Plasma alcohol concentration was carried out using the BioVision Ethanol

Colorimetric Assay Kit (BioVision incorporation, Milpitas, USA) according to the manufacturer's instructions. All reactions and readings were done in an alcohol-free environment using iMark Bio-rad Microplate Absorbance Reader (Bio-rad Laboratories Inc, USA). The protocol followed is shown in appendix 2.

The BioVision Ethanol Colorimetric Assay kit provides rapid, simple, and sensitive method for accurate quantification of ethanol concentration in samples such as serum, plasma, food, beverages and other growth media. The ethanol is acted upon by alcohol oxidase to generate hydrogen peroxide (H_2O_2) that subsequently reacts with the kit's probe to generate colour $\lambda max = 570$nm that was measured using a micro-plate reader. The kit detects alcohol level of 0.1 -10mg/dl.

2.3 Bone decalcification

Left tibiae were rinsed in distilled water to remove excess formalin and then individually immersed in disodium ethylenedeamine tetraacetic acid (EDTA) approximately 20 times the bone volume for three weeks (Appendix 3). Solutions such as: morse solution, 5% trichloroacetic acid, formic acid, and hydrochloric acid were used previously for decalcification. These solutions were found to have negative effects on preservation of tissue morphology, antigenicity and DNA integrity. In contrast, EDTA is widely used in immunolocalization because of its ability in tissue antigenicity preservation. However, it requires a longer decalcification time taking several weeks or months (Castania et al., 2015).

2.4 Test for end point decalcification

To test for end point decalcification, 5mls of EDTA covering the specimen was drawn and placed into a separate tube. About 10mls of ammonium oxalate was added to the same test tube. The mixture was left to stand overnight and then observed for precipitate (Appendix 4). The absence of precipitate indicated complete decalcification of the respective bone. All bone samples were rinsed in slow running tap water for 30 minutes and then placed in fresh 10% buffered formalin for three weeks before further processing.

2.5 Bone length measurement

Prior to processing, the length of the individual bones was measured using a digital caliper. The use of digital caliper affords simple and accurate measurement of 0.01mm or even better. Bone tissue was placed in a flat surface and the two internal jaws of the caliper slightly touching the proximal and distal ends of the bone as the reference points. Each measurement was repeated until a consistent result was achieved. The value was then divided into three equal parts representing the length of the shaft, proximal and distal ends. The exact length of the proximal end was measured and carefully separated from the shaft for subsequent processing and embedding.

2.6 Tissue processing

The proximal end of the tibiae was then processed overnight in an automated tissue processor (Shandon Citadel 1000) as follows: fixation in 10% buffered formalin for 4 hours, dehydration in 70% alcohol each for 1 hour, in 3 changes of 95% alcohol for 2

hours each, in 3 changes of 100% alcohol for 2 hours each, in 2 changes of chloroform for 2 hours each and then impregnation in two changes of paraffin wax for 2 hours each (Appendix 5).

2.7 Paraffin wax embedding

Tissue samples were then embedded in paraffin wax making sure that the anterior surface of the proximal end of the tibia was aligned in contact with the floor of the mold using forceps. The embedding wax, forceps and the molds were preheated at a temperature of 60°C. Tissue samples were positioned in the metal molds, filled with molten wax and then covered with labelled plastic cassettes. The wax blocks were then allowed to cool on a frosted surface for about 20 minutes (Appendix 6), before they were removed from the molds.

2.8 Sectioning

Excess wax surrounding the block was trimmed using a blade. When trimming, care was taken to ensure that the upper and lower horizontal edges were parallel to each other. The blocks were then cut to the level of the tissue with the microtome. One corner was trimmed off to keep the ribbon straight during sectioning and to recognise the leading end of the ribbon (Fig. 2.3).

The blocks were cooled on ice before cutting 5µm thick sections. A ribbon of 9 sections was cut after discarding the first 20 sections. To flatten the tissue sections the ribbons of wax were floated in a preheated water bath at 45°C.

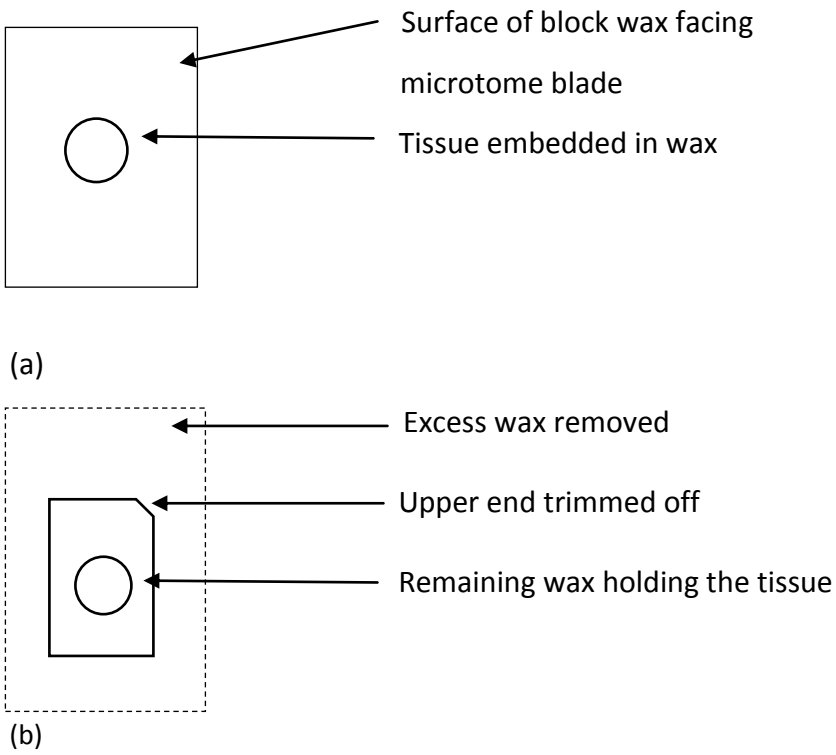

Figure 2.3: Trimming of wax blocks: (a) the surface of wax block facing the microtome blade before trimming; (b) excess wax removed and upper left corner trimmed off to determine the leading end of the ribbon.

Once flattened in the water bath, forceps were used to separate the sections. The individual sections where then mounted onto silane coated microscope glass slides in a sequential order (Fig. 2.4).

The first section was stained with hematoxylin and eosin (H&E); every alternate second and third section was immunolabeled with the anti-Ki-67 antibody and its negative control, respectively. This process was repeated after discarding the first 20 sections and hence each experiment done in duplicate.

Slides were dried at room temperature and then stored in an oven at 37°C**.** The oven heated the slides and melted the wax surrounding the tissues. Sections where then allowed to dry further until particular stain was conducted.

1 H&E	2 Ki-67	3 Neg	4 H&E	5 Ki-67	6 Neg	7 H&E	8 Ki-67	9 Neg

(a)

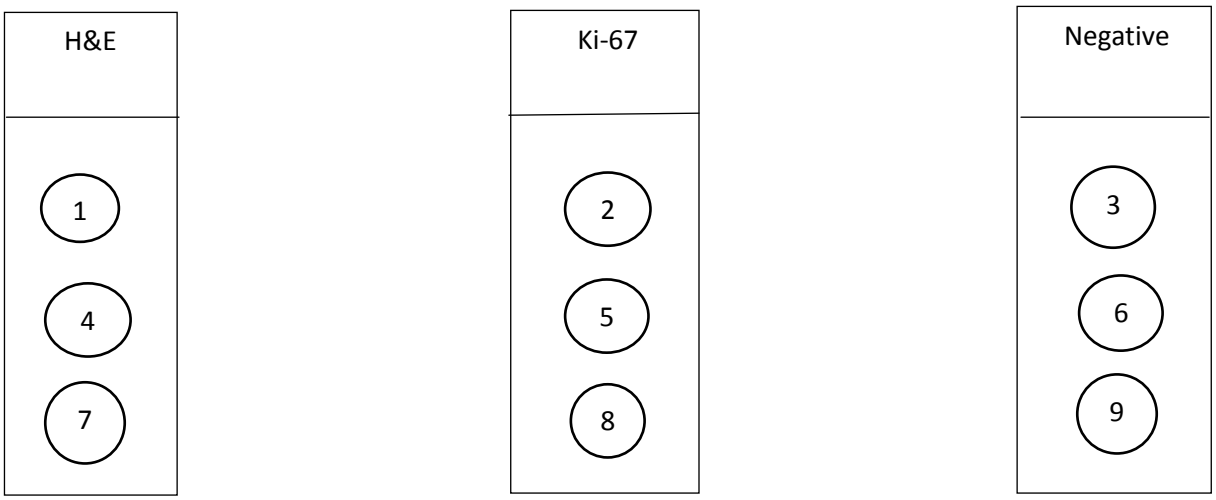

(b)

Figure 2.4: Serial sectioning of tissue. (a) The manner in which ribbons were serially sectioned **(b)** the way in which slides were labelled and sections were picked.

Silane coated slides were used to supplement the adhesive property of the tissue sections to the slides. The following procedure was used in coating the slides: slides were organized in a rack and completely immersed in 2% 3-aminopropyltriexothysilane (APES) for 30 minutes, rinsed in 2 changes of acetone for 10 dips, rinsed in 2 changes of

distilled water for 10 dips, and then air dried at a 45^0 angle. Slides were then incubated overnight at 37^0 (Appendix 7).

2.9 Staining of tissue sections

Haematoxylin and eosin staining

The haematoxylin and eosin stain is used to determine the structural organization of tissue. Haematoxylin stains the nuclei blue/black, while the eosin gives cytoplasm and connective tissue pinkish and red colours respectively. This differentiates between the nuclear and non-nuclear components of the cell. Sections were initially dewaxed in xylene for 2x 10 minutes and rehydrated by passing them through series of decreasing alcohol concentration (100%, 95%, and 70%) for 3 minutes each and eventually rinsed in distilled water for 5 minutes. The sections were then stained with haematoxylin for 10 minutes, washed in running tap water for 2 minutes, differentiated in periodic acid for 2 dips, rinsed in slow running tap water for 2 minutes, blued in Scott's tap water for 2 minutes and then rinsed again in tap water for 10 minutes. Sections were stained with eosin for 2 minutes for cytoplasm staining and then dehydrated with increasing concentration of ethanol (70%, 95%, and 100%) for 3 minutes each, cleared in 2 changes of xylene for 10 minutes each and finally mounted in entellen (Appendix 8.1).

The use of Scott's tap water is associated with gentle and smooth bluing of haematoxylin and decrease loss of tissue sections. The water was prepared by dissolving 2g of sodium hydrogen carbonate and 10g of magnesium sulphate in one

liter of distilled water. The solutions were then stored in room temperature (Appendix 8.2).

Ki-67 Immunohistochemistry (IHC)

Chondrocyte proliferation is an intergral part of bone development. The anti-Ki-67 antibody (ab6246212 abcam) has received great attention as a marker for cellular proliferation. The antibody was found to be reactive with nuclear structures present only in proliferating cells. This procedure was carried out over a period of three days using the Rabbit Specific HPR/DAB (ABC) detection IHC kit (ab624621 ABCam) as per manufacturer's instructions. The first day of the procedure comprised of dewaxing (2x 5 minutes) and rehydrating the tissue sections, washing tissue sections in running tap water for 5 minutes. The slides were then immersed in staining rack filled with citrate buffer solution (pH=6) and kept in a water bath set at temperature of 60^0C. The high temperature and the calcium chelating by citrate is found to destroy the protein complex formation in formalin fixed tissue thereby unmasking the specific epitopes within the protein molecules for effective antigen-antibody reaction (Shi et al., 2001).

The second day, tissue sections were allowed to cool to room temperature for 20 minutes and then washed in phosphate buffer solution (PBS) (pH=7.4) for 5 minutes. Endogenous peroxidase was blocked with 1% hydrogen peroxide (H_2O_2), washed with PBS for 3x 5minutes, incubated with normal goat serum for 10 minutes, incubated with primary antibody (ki-67 in 1:1200 dilution factor) overnight at 4^0C. Endogenous peroxidase is an enzyme (produced by most tissues) that can produce nonspecific

staining background. Although the enzyme activity is known to be destroyed during fixation, treatment of tissue section with 1% H_2O_2 will further reduce or completely abolish the nonspecific staining background (Ramos-Vara, 2005).

The third day, sections were allowed to reach room temperature, washed in PBS for 3x 5 minutes, incubated with biotinylated secondary antibody, washed in PBS for 3x 5 minutes, incubated with streptavidin HRP, washed in PBS for 3x 5 minutes. Sections were then incubated with 3-3' di-aminobenzidine (DAB) working solution for 5 minutes, rinsed in running tap water for 5 minutes, hydrated through graded alcohol, cleared in xylene and eventually mounted in entellen (Appendix 8.3).

Use of streptavidin in immunohistochemical staining has been shown to inhibit the action of biotin. Biotin is widely produced by many tissues including bones and can produce nonspecific staining background. It can also bind to the antibodies or the enzyme epitopes used in detecting target antigen. Streptavidin has a high affinity to the biotin thereby inhibiting the interaction and abolishing the nonspecific staining background (Ramos-Vara, 2005).

2.10 Light microscopy and photomicrography

A light microscope (Zeiss Axioscope 2 plus) fitted with an axiocam HRC digital camera was used to take Photomicrographs of the stained slides. These were taken on the medial, lateral and central region of each section under ×10 magnification. From these photomicrographs an assessment of chondrocyte number, cellular proliferation and the

area of the chondrocytes zones (proliferative and hypertrophic) of the proximal growth plates were done.

Photomicrographs were imported into Fiji Image-J software and the parameters measured were delineated based on cell morphology. The proliferative zone is delineated by the first flattened chondrocyte on the epiphyseal end and the first hypertrophic chondrocyte on the metaphyseal side. Whilst the hypertrophic zone is delineated by the first hypertrophic chondrocyte from the epiphyseal side and by the last transverse septum on the metaphyseal side (Fig. 2.5). Absolute parameters assessed include the following: cell count, cellular area, growth plate area, as well as cellular proliferation.

Cell count

Cell count was determined as the average number of cells within each zone of the growth plate (proliferative and hypertrophic zone) as follows: images were converted to greyscale (8-bit) after which the area of the cells to be counted was highlighted. This was done using the "set" button to type in a known pixel intensity thereby creating a binary version of the image with two pixel intensities: black = 0 and white = 255. For merged cells, process > binary > watershed, and fill holes was used to accurately separate them by adding one-pixel cell line and fill holes respectively. The region of interest (ROI) was selected and particles were analysed. To count all the particles, setting was adjusted to the default of 0-infinity. Finally, an outline choice shows a copy

of the image and all counted particles as well as the cellular area were shown in numbered outlines (Appendix 9.1).

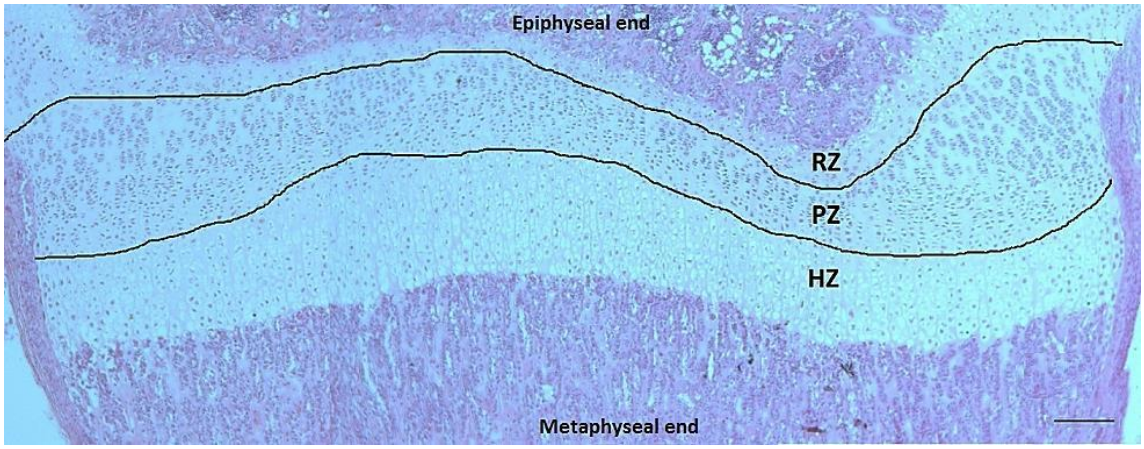

Figure 2.5: Photomicrograph of the growth plate showing the resting, proliferative and hypertrophic zones. Proliferative zone (PZ) and hypertrophic zone (HZ) areas (irregular lines) are delineated. Haematoxylin and Eosin (Image courtesy of Bello NK and Perry V).

Cellular area

Cellular area was determined as the average sum of the area occupied by the cells in each zone (proliferative and hypertrophic zone) as explained above.

Growth plate area

Growth plate area was determined as the average sum of the resting, proliferative and hypertrophic zones area. Following the automated routine threshold setting as explained above, the entire growth plate area was selected using a polygonal selection tool. An outline of the analysed area was drawn and summarised.

Cellular proliferation

Cellular proliferation was determined as the average number of Ki-67 positive cells within the proliferative and hypertrophic zones of the growth plate as described above.

2.11 Three-dimensional micro-focus x-ray computed tomography (3D-µCT)

Recently, high-resolution 3D imaging technique has received much attention in evaluating bone morphology and microarchitecture. It involves the use of X-ray attenuated data that is acquired at multiple viewing angles to reconstruct a 3D representation of the specimen. The accuracy and non-destructive advantages of assessing bone morphometry by µCT makes the specimen useful for other subsequent assays (Bouxsein et al., 2010).

The samples preserved in 10% buffered formalin were first freed of excess fluid by patting around the bone with a paper towel prior to scanning. The bones were then individually wrapped in styroform and placed in a plastic container. Wrapping styroform around the bone ensured that the sample remained stationary during scanning while allowing the X-rays to get to the sample with negligible absorption. The plastic container with the sample inside was then positioned on a rotating manipulator in the scanning chamber for the scanning. The scanning parameters used are shown in table 2.1.

Table 2.1: Scanning parameters

Parameter	Value
X-ray voltage	70kv
X-ray current	400µa
Filter	1mm aluminum
Scanning resolution	15µm
Tomographic rotation	360 degrees
Rotation step	1 degree
Frame averaging	4
Scan duration	8 minutes

Parts of the tibia studied

The full bone length was measured using the VG studio built in caliper. Cross-sectional area, cortical area and medullary canal area of the shaft were measured at two positions, 50th (midshaft) and 25th (proximal) percentile marks of the tibial length (Fig. 2.6). These points were determined by dividing the bone length into quartiles. From the midshaft, the circumference was also taken.

Table 2.2: Trabecular parameters assessed

Parameter	Definition
$\frac{BV}{TV}$ (bone volume to total volume)	Represents the ratio of material (bone) volume to total volume.
TbTh (mean trabecular thickness)	Specifies the mean thickness of trabecular (column-like) structures in the material (bone), calculated as follows: $\mathrm{TbTh} = \frac{2}{\frac{BS}{BV}}$ *Where* $\frac{BS}{BV}$ *is the ratio of material (bone) surface (BS) to material (bone) volume (BV).*
TbN (mean trabecular number)	Shows the mean number of trabecular (column-like) structures per unit length, calculated as follows: $\mathrm{TbN} = \frac{\frac{BV}{TV}}{\mathrm{TbTh}}$
TbSp (mean trabecular spacing)	Indicates the mean distance between trabecular (column-like) structures, calculated as follows: $\mathrm{TbSp} = \frac{1}{\mathrm{TbN}} - \mathrm{TbTh}$

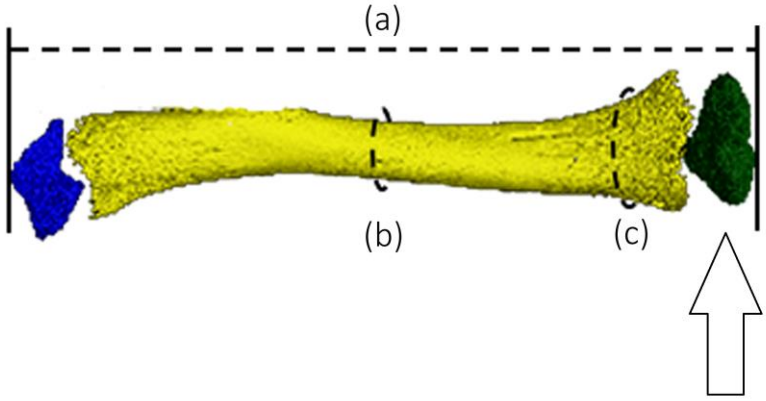

Figure 2.6: Three-dimensional reconstruction of the tibia showing the parts that were investigated. (a) full tibial length; (b) 50th percentile mark (midshaft); (c) 25th percentile mark. The green part represents the proximal epiphysis in which trabecular morphometric were studied. The yellow part is the midshaft (Image courtesy of R. Ndou).

Bone morphometry

Reconstruction was done using 3D Pro® after which, VG studio Max® 3.0 was used for data analysis. An import histogram was used to exclude the gray values representing the container. On the preview, the parts representing air were also cut out to reduce computer memory processing power required during analysis. Care was taken to ensure the sample was not cut out. To ensure that only the bone material was being examined, manual surface determination was applied confirming that the background was removed without compromising the sample material of interest. The region of interest was then selected for surface determination. After selecting the proximal epiphysis as a region of interest, the trabecular number, thickness, spaces and volume were obtained under “morphometrics” on VG studio.

Osteometric measurements were obtained using the built-in caliper. The full bone length was divided to determine the midshaft and further divided into four to determine the quartile marks. A cross sectional slice from each quartile was then saved for further analysis on Fiji image J. From these slices, cross sectional circumference, cross sectional area and cortical thickness where obtained as described in appendix 9.2. Cortical thickness was the difference between the cross-sectional area and the medullary cavity area.

2.12 Statistics analysis

The data were managed in Microsoft Excel 2016 (Microsoft Corporation) and analyzed using SPSS® version 24, IBM®, 2017. The Shapiro Wilks test was used to test for normality. Since the data were parametric, ANOVA with LSD post-hoc was used to test for group differences. Pearson's correlation was used to test for relationships between parameters. Binary logistic regression was used to predict group membership into either the ethanol or saline control group. Principal Component Analysis (PCA) was conducted to determine the parameters that contribute the most into group membership. The data are reported as mean ± standard deviation. Significance level was set at $p < 0.05$.

CHAPTER 3: RESULTS

3.1 Measurement reliability

Lin's concordance correlation coefficient (p_c) for intra and interobserver errors showed p_c values above 0.7 for all measurements. Values for pc range from -1 to 1 and a value close to 1 indicates a high degree of measurement similarity. Greater than 0.7 pc values obtained herein indicate that the correlation between repeated measurements was high and thus measurement error was minimal.

3.2 Blood alcohol concentration

The mean blood ethanol concentration in the experimental group (n=6) was 258.77 mg/dL and 81.53 mg/dL in the saline controls. The untreated controls were not tested for blood ethanol concentration as they did not receive treatment.

3.3 Food consumed and weight gained during the gestation period

All three groups studied showed similar daily food consumption in each week. The food intake was highest in week 3 for all the groups, and was not significantly different between the groups (p=0.75 for ethanol vs saline control) (Fig. 3.1). With respect to the weight gained per week, the ethanol group showed a negligible gain from week 1 (28.3g) to week 2 (29.42g). In contrast, the saline and untreated controls exhibited a slight weight decrease from week 1 to week 2 (34.21g – 29.21g and 30.5g – 24.83g respectively). However, all the three groups showed a major weight increase from week 2 to week 3 (Fig. 3.2). The ethanol group had the least total weight gained for the entire gestation period (Fig. 3.3).

3.4 Gestation duration and litter size

The gestation duration ranged from 19 to 24 days (Table 3.1). This range was 21-24 days in the ethanol group and 19-23 days in the saline controls. The untreated controls had 23 days gestation. However, there were no statistical group differences in gestation duration (p=0.37 for ethanol vs saline control). There was a wide range of litter size among the three groups, with the smallest being 3 in the ethanol group and the largest observed in the untreated controls that had a maximum of 17 (Table 3.1). This group also had the smallest range of 14 -17. These contrasts with the ethanol group (litter size 3-16) and the saline controls (litter size 5-16). However, there were no significant differences found between the groups (p=0.28 for ethanol vs saline control). Each of the three groups in the study had 2 pups found dead at birth.

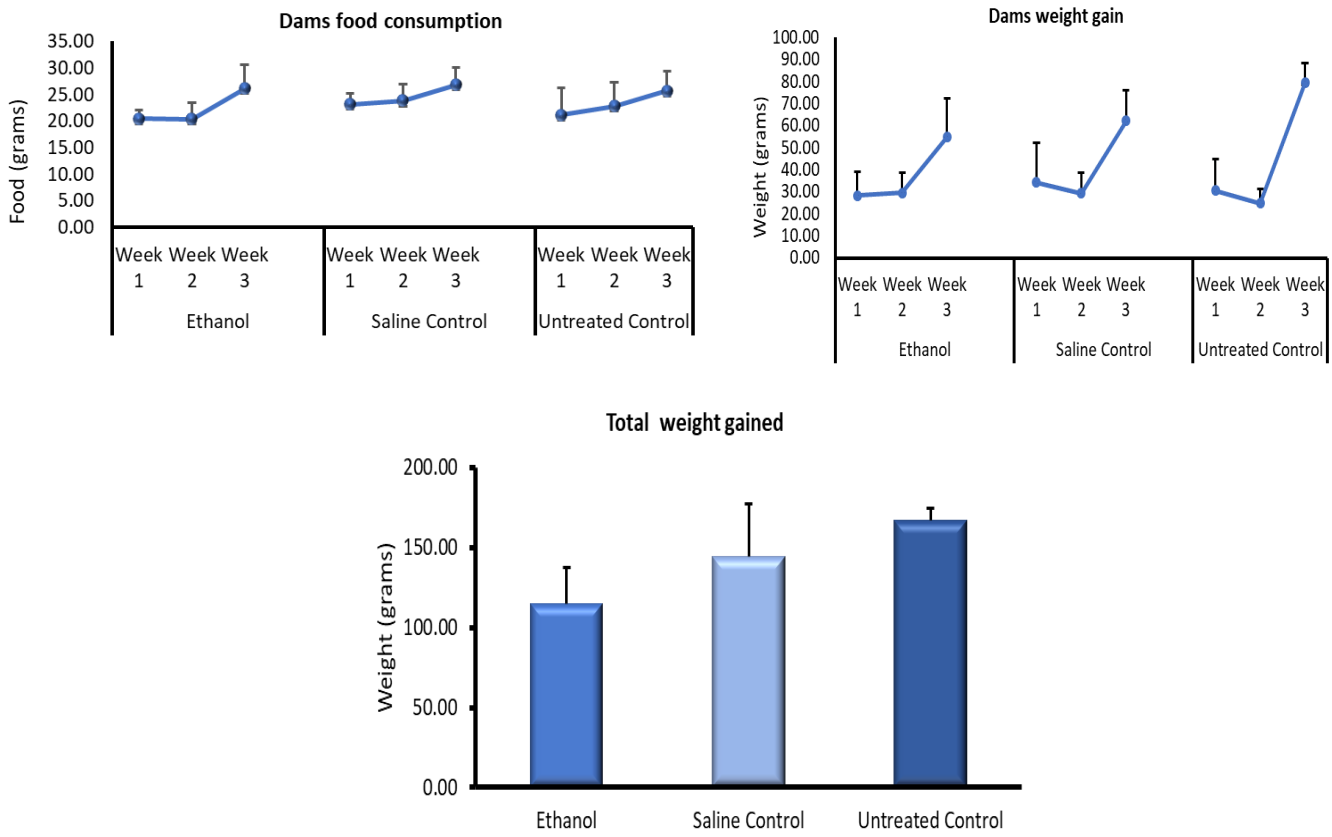

Figure 3.1: (a) Food consumption. The daily food consumption in grams is shown as an average per week for all three groups in the study. Error bars represent standard deviation (b) **Weight gain. T**he weekly mean weight gained in grams is shown for all three groups in the study. Error bars represent standard deviation (c) **Overall weight gain**. The total mean weight gained in grams for the entire gestation period is shown for all three groups in the study. Error bars represent standard deviation.

Table 3.1: Gestation duration and litter size for the ethanol group, saline and untreated controls. The number of dead pups (n = 2) in each group is included in litter size.

Group		N	Minimum	Maximum	Mean	SD
Ethanol	Gestation	6	21	24	23.00	1.095
	Litter size	6	3	16	9.83	4.916
Saline Control	Gestation	6	19	23	22.00	1.732
	Litter size	6	5	16	12.14	3.671
Untreated Control	Gestation	3	23	23	23.00	0.000
	Litter size	3	14	17	15.33	1.528

3.5 Pups weights and crown rump length at 3 weeks of age

Minor differences in the weight of the pups at the age of 3 weeks were observed. The ethanol group (47.41g) weighed marginally lower than the saline (48.20g) and untreated controls (50.83g) (Fig. 3.4). These differences were not statistically significant (p=0.45). The crown rump length was similar in the ethanol group and the saline controls (9.70cm), being significantly higher in the untreated control group (p=0.01 for untreated control against the ethanol and saline groups) (Fig. 3.5)

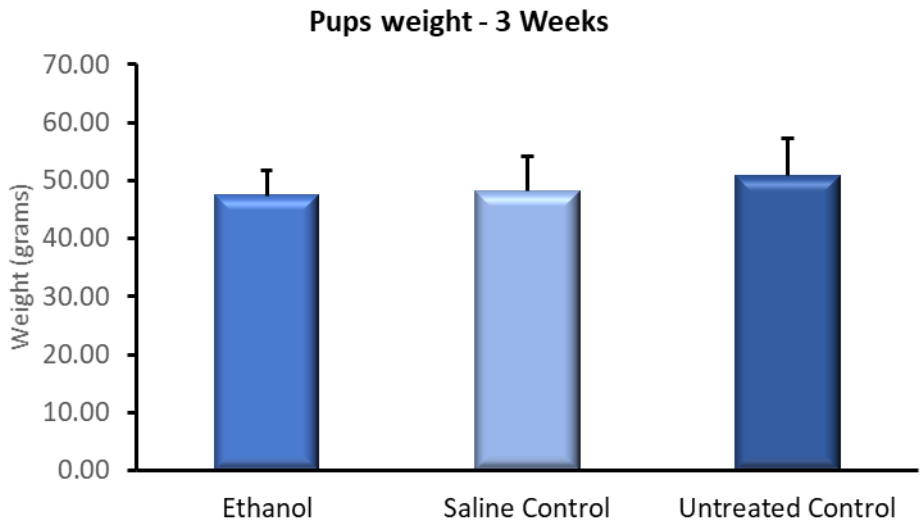

Figure 3.4: Weight of the pups at 3 weeks of age. The mean weight is given in grams for all three groups in the study. Error bars represent standard deviation.

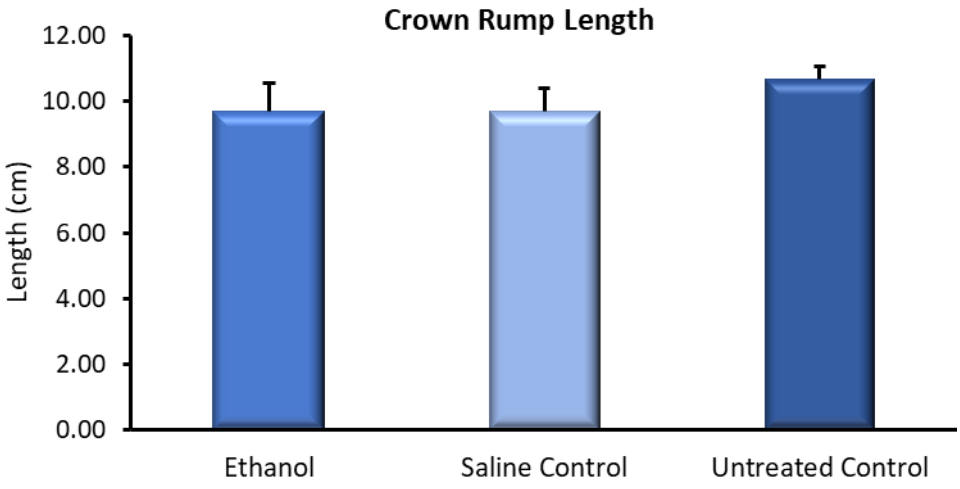

Figure 3.5: The crown rump length of the pups at 3 weeks of age. The values are means in cm for all three groups in the study. Error bars represent standard deviation.

3.6 Histomorphometry and immunohistochemistry for Ki-67 protein

Epiphyseal plate surface area

The epiphyseal plate surface area was smallest in the ethanol group (Mean=9.48 mm^2 ±1.53) compared to the saline (Mean=10.70 mm^2 ±1.63) and untreated controls (Mean=12.07 mm^2 ±0.47). These differences were significant between the ethanol and untreated controls (p=005) (Fig. 3.6a).

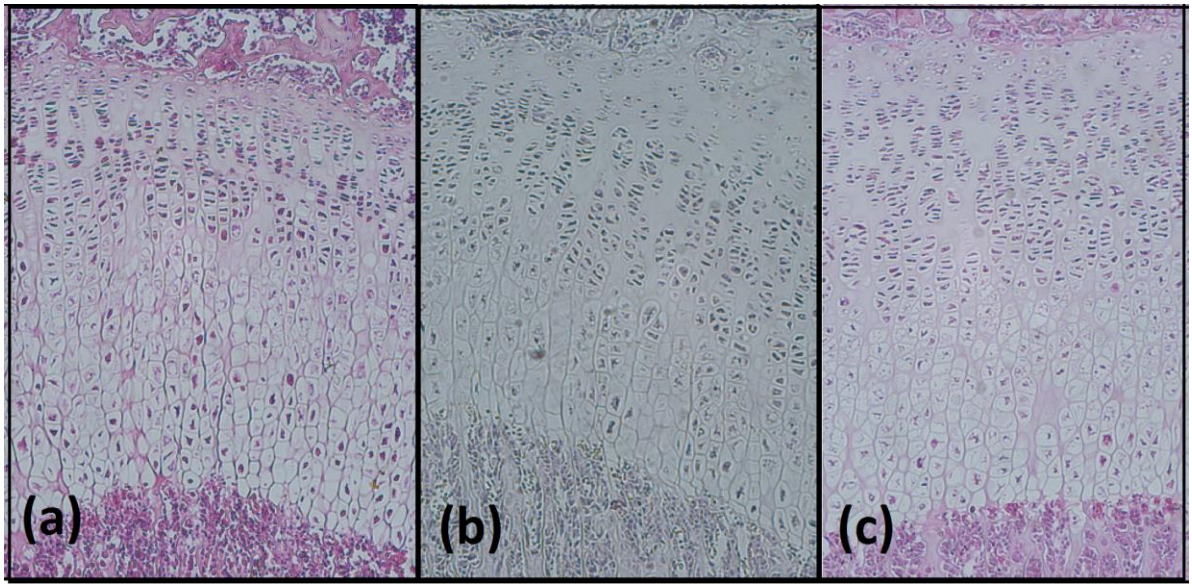

Figure 3.6: Representative photomicrographs of the Haematoxylin and Eosin stained section for the three groups. (a) Ethanol (b) Saline Control and (c) Untreated Control.

Proliferative zone

The ethanol group exhibited fewer cells (Mean=1788.01 ±408.45) than the saline and untreated controls (Mean= 2244.36 ±480.99 and 2325.64 ±793.17, respectively).

However, no significant differences were observed among all three groups ($p>0.05$) (Fig. 3.6b). This group also had the smallest proliferative zone surface area Fig (3.6c). While no significant differences were observed between the ethanol and saline control group ($p=0.34$), there was a statistically significant difference between the ethanol (Mean=0.26mm^2 ±0.05) and the untreated group (0.57 mm^2 ±0.16) ($p<0.001$). Similarly, fewer Ki-67 labeled cells were found in the ethanol group with significant differences between the ethanol (Mean=1691.30 ±535.91) and the untreated group (Mean=2863.25 ±1613.79) ($p<0.038$) (Fig. 3.6d).

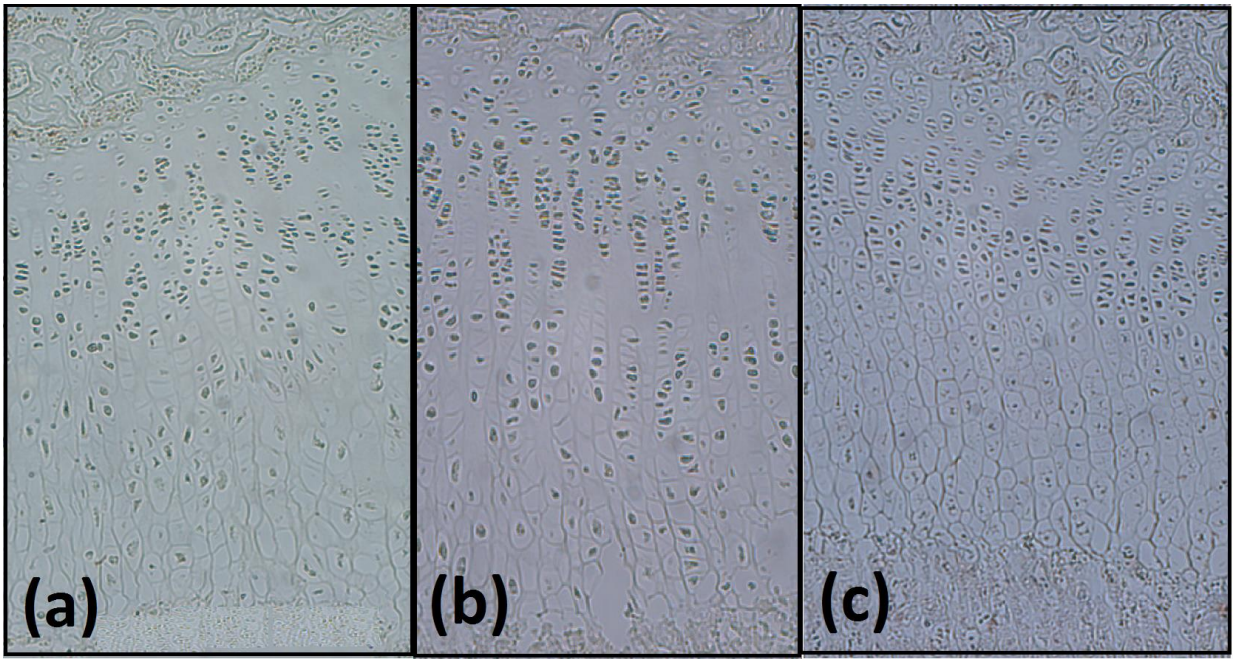

Figure 3.7: Representative photomicrographs of the Ki-67 Immunohistochemistry stained sections for the three groups. (a) Ethanol (b) Saline Control and (c) Untreated Control.

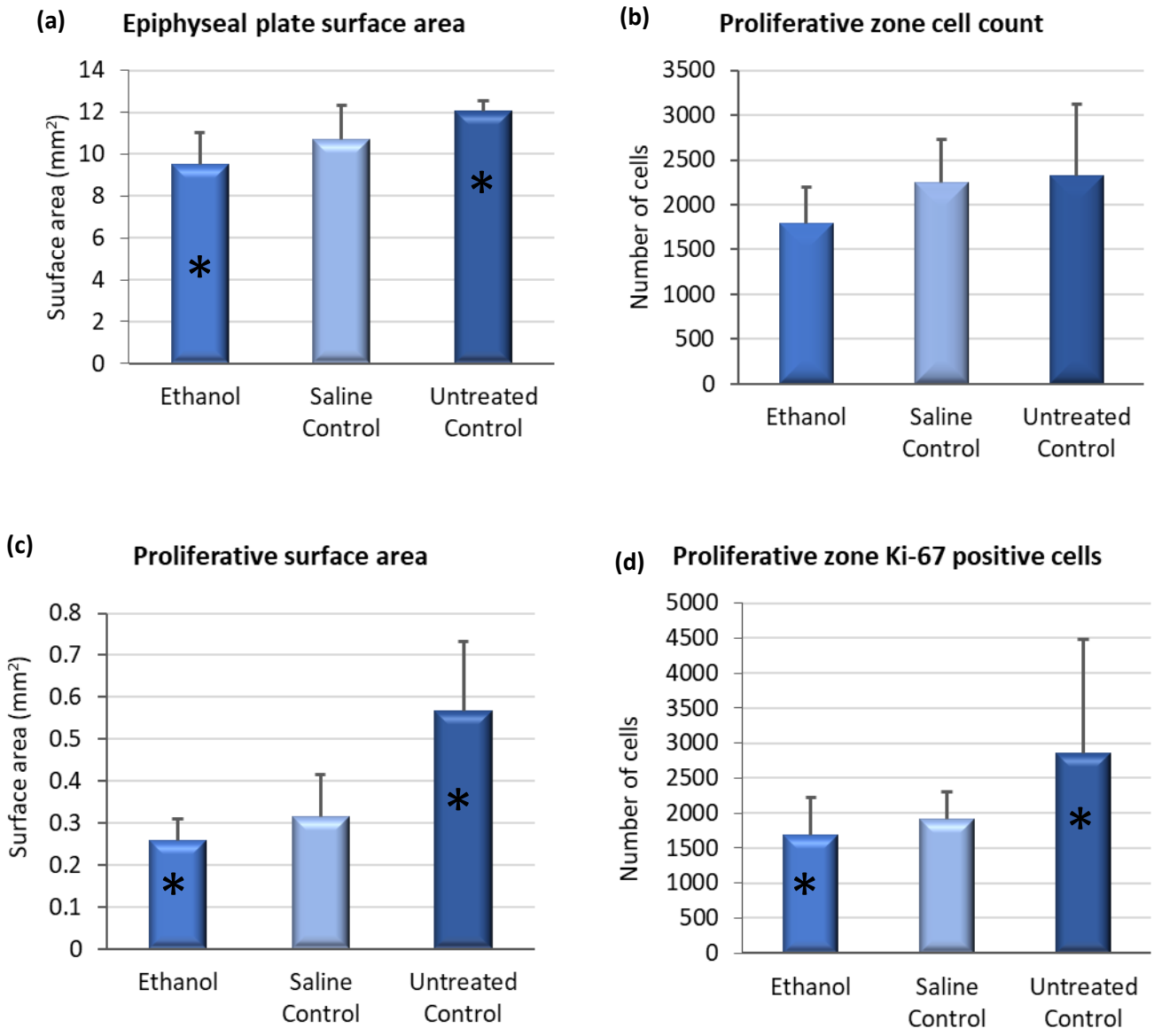

Figure 3.7: Histomorphometry and Ki-67 positive cells in the tibia proximal Epiphyseal plate proliferative zone. (a) epiphyseal surface area, (b) proliferative zone number of cells (c), proliferative zone surface area and (d) the number of Ki-67 positive cells in the proliferative zone are given for the ethanol, saline control and untreated control groups (Error bars represent standard deviation and stars indicate statistical significance).

Hypertrophic zone

In the hypertrophic zone, the ethanol group had fewer cells (Mean=1275.20 ±202.18) than the saline controls (Mean=1935.17 ±323.78) and the untreated group (Mean=2654.58 ±445.17) ($p<0.001$ for all group comparisons) (Fig. 3.7a). The ethanol group also had the smallest (Mean=0.17 mm^2 ±0.05) hypertrophic zone surface area compared to the saline (Mean=0.30 mm^2 ±0.14) and untreated controls (Mean=0.39 mm^2 ± 0.19). However, significant differences only occurred between the ethanol and the untreated group ($p>0.006$) (Fig. 3.7b). In this zone, Ki-67 positive cells were fewer in the ethanol (Mean=1081.19 ±207.14) compared to the saline controls (Mean=1646.83 ±434.99 and untreated group (Mean=1157.25 ±232.37). However, these differences were not statistically significant ($p>0.05$) (Fig. 3.7c).

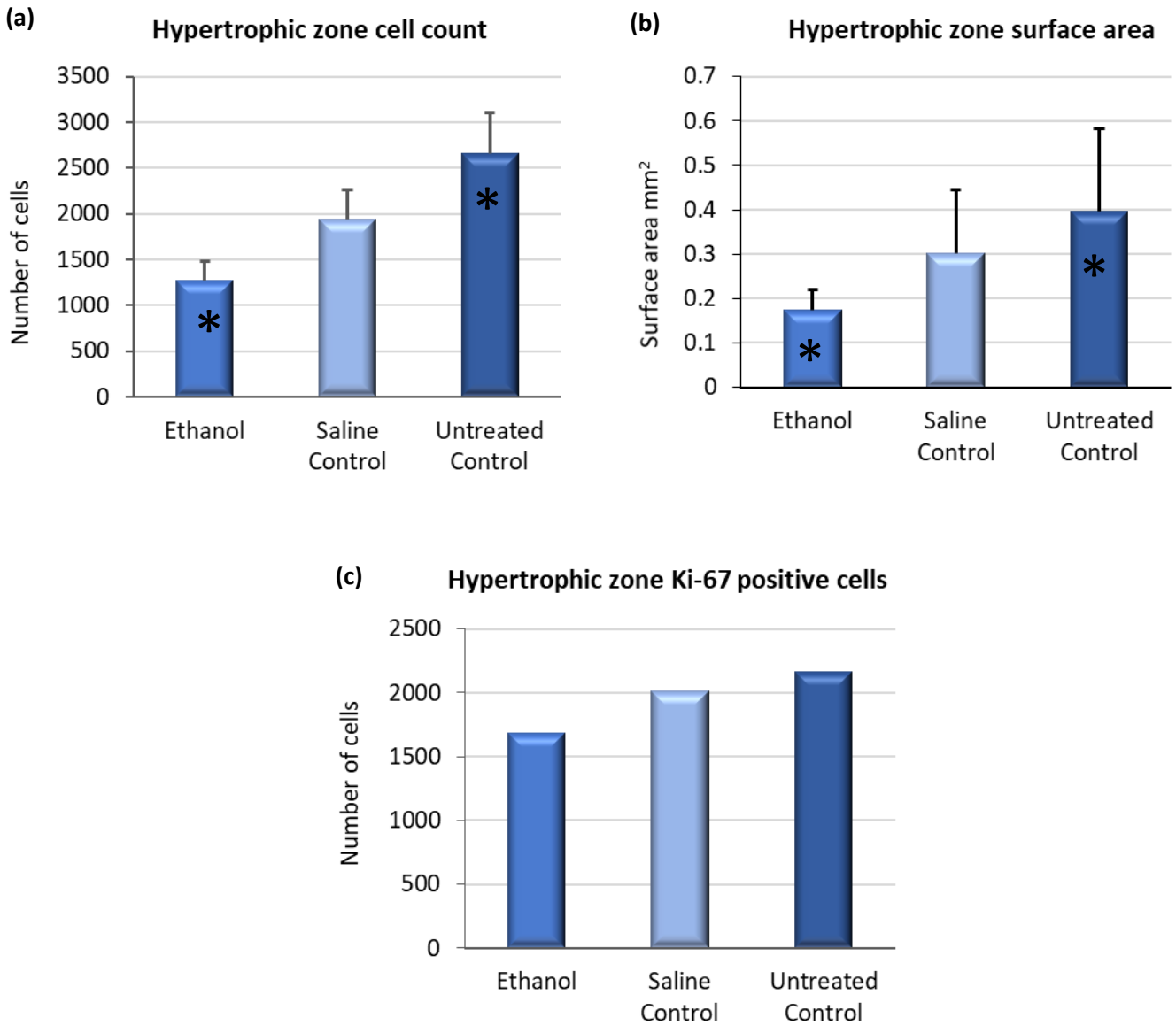

Figure 3.7: Histomorphometry and Ki-67 positive cells in the tibia proximal epiphyseal plate hypertrophic zone. (a) Number of cells, (b) surface area and (c) the number of Ki-67 positive cells in the hypertrophic zone are given for the ethanol, saline control and untreated control groups. (Error bars represent standard deviation and stars indicate statistical significance).

3.7 Osteometry

The mean full bone length was similar in all three groups studied (ethanol, mean=21.08mm ±0.95; saline control, mean=21.23mm ±1.38 and untreated control, mean=21.88mm ±0.94) (Fig. 3.8a). This similarity among the groups was also observed in the shaft length. The mean shaft length for the ethanol group was 17.77mm ±0.92 and 17.51mm ±1.32 for the saline and untreated controls a mean of 18.22mm ±0.74 (Fig. 3.8b). In contrast, the proximal volume showed differences between the study groups, with the ethanol group showing a significantly smaller volume (Mean=3.51mm^3 ±1.07) than the saline (Mean=4.35 mm^3 ±0.78) and untreated controls (Mean=4.26 mm^3 ±1.02) ($p=0.007$ and $p=0.04$ for the ethanol group compared to the saline and untreated groups respectively) (Fig. 3.8c).

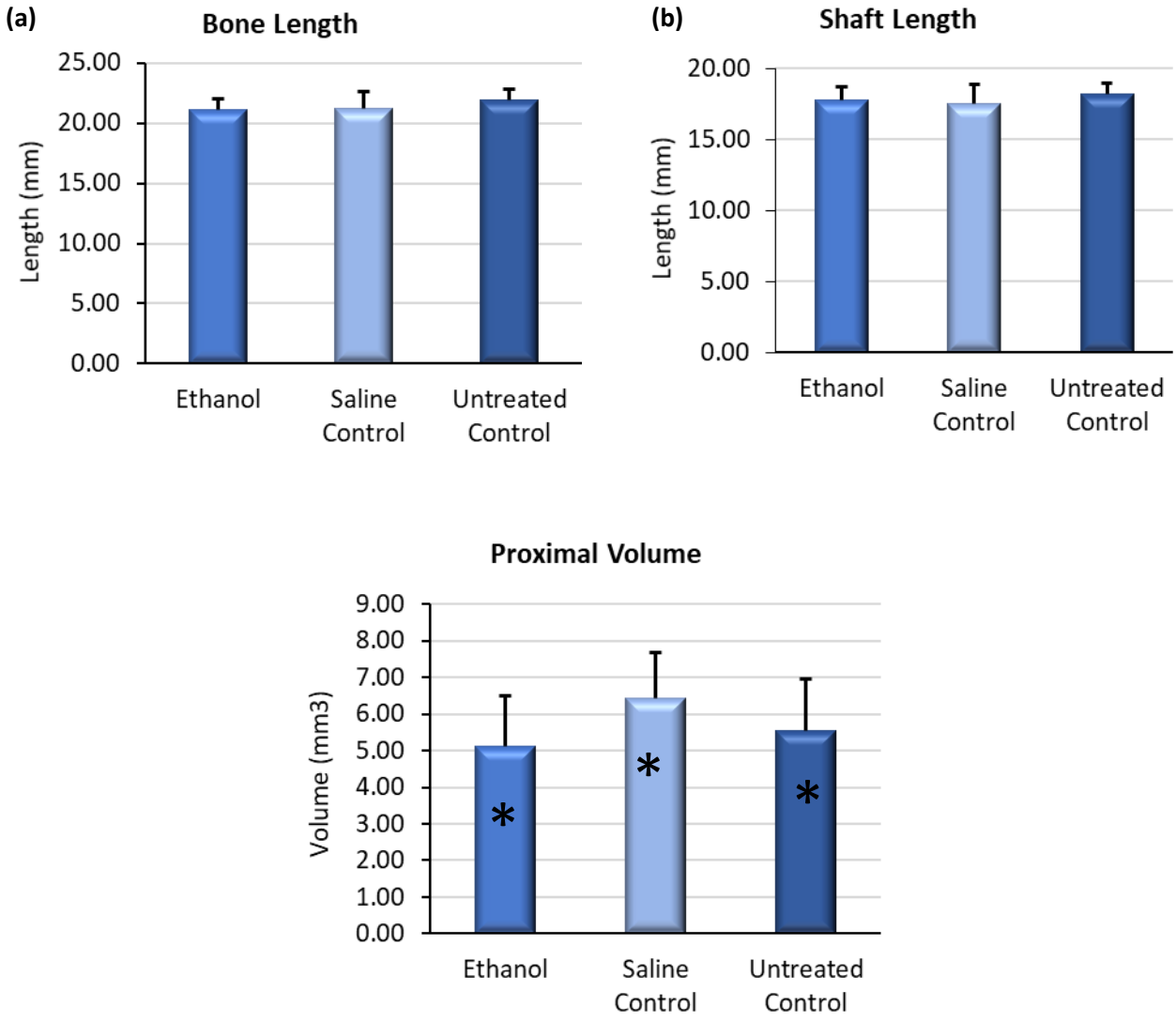

Figure: 3.8: Measurements and volume. (a) Full bone length, (b) shaft length and (c) proximal volume. All parameters are given for the ethanol, saline controls and untreated controls. (Error bars represent standard deviation and stars indicate statistical significance).

Trabecular parameters

The ethanol group (Mean=51.86% ±8.62) also had less bone to total volume (BT/TV) compared to the saline (Mean=61.34% ±10.30) and untreated controls (Mean=56.44 % ±9.58) (Fig. 3.9a). This difference was significant for the ethanol and saline groups

(p=0.03) with both control groups showing similarity (p=0.38). The ethanol group (Mean= 0.10 ±0.06) showed the thinnest trabeculae (TbTh) of all three groups in the study, being significantly lower than the saline (Mean= 0.19 ±0.10) and untreated group (Mean=0.20 ±0.11) (p=0.04 and p=0.05 compared to the ethanol group respectively) (Fig. 3.9b). The number of trabecular (TbN) was similar in all three groups (ethanol, Mean=4.71 ±1.49; saline control, Mean= 4.67 ±1.01 and untreated control, Mean= 5.04 ±0.94) (Fig. 3.9c). Trabeculae spacing (TbSp) was similar among the groups, with the ethanol group showing a Mean of 0.11mm ±0.07, saline controls Mean=0.10mm ±0.02 and untreated group (Mean=0.14mm ±0.03) (Fig. 3.9).

Proximal cross-sectional area, cortical area (thickness) and medullary canal area

The proximal cross-sectional area was marginally lower in the ethanol group (4.81 mm^2) compared to the saline and untreated controls that had the same size area (5.10 mm^2). Although the ethanol group appeared to have a smaller cross-sectional area in this bone region, it was not significantly different from the controls (p=0.57) (Fig. 3.10). Conversely, a greater medullary canal area occurred in the ethanol group (3.02mm) in comparison to the saline and untreated controls (2.84mm^2 and 2.58 mm^2 respectively). These differences were only significantly different between the ethanol group and untreated controls (p=0.05) (Fig. 3.11). With respect to cortical area (thickness) in this bone region, the ethanol group (1.79 mm^2) exhibited a marginally lower value compared to the saline and untreated controls (2.21mm^2 and 2.48 mm^2 respectively). Again, these differences were not significantly different (p=0.17) (Fig. 3.12)

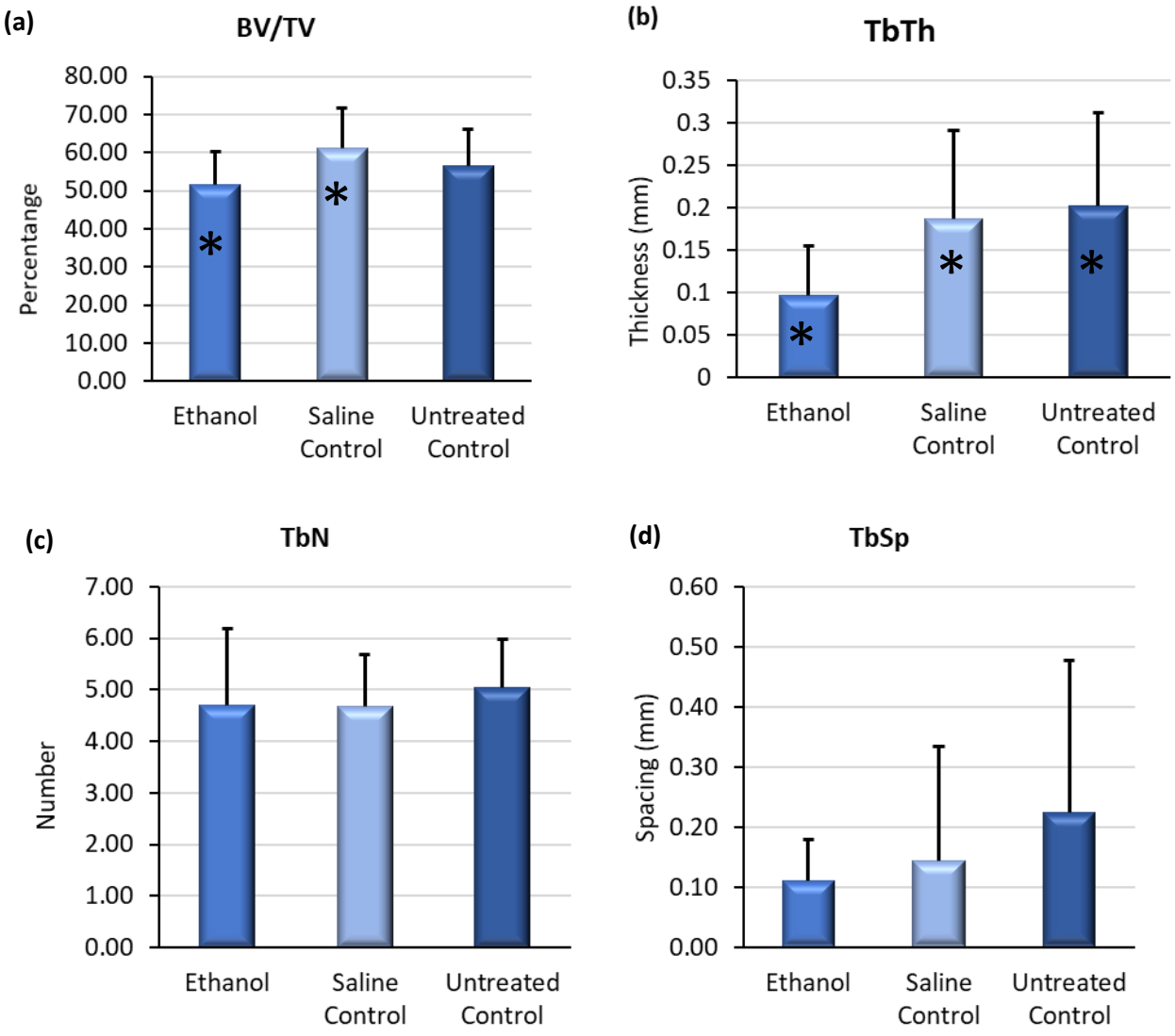

Figure 3.9: Trabecular morphometric parameters (a) Bone volume to total volume (BV/TV), (b) trabecular thickness (TbTh), (c) trabecular number (TbN), (c) trabecular spacing (TbSp). All parameters are given for the ethanol, saline controls and untreated controls. (Error bars represent standard deviation and stars indicate statistical significance).

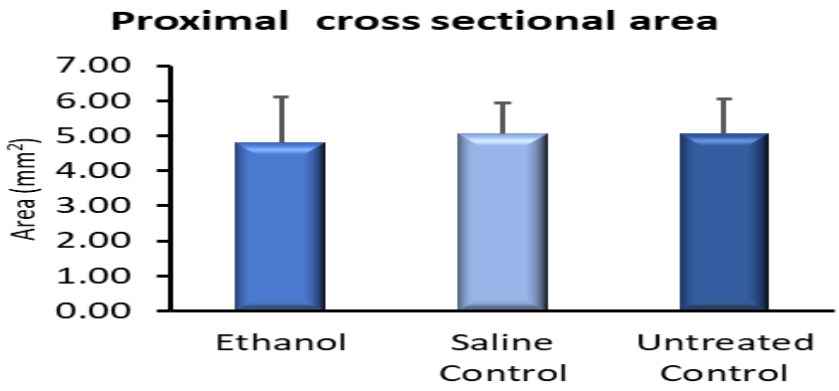

Figure 3.10: Proximal cross-sectional area. The mean bone cross sectional area at the 25th percentile mark is given for the three groups studied. Error bars represent standard deviation.

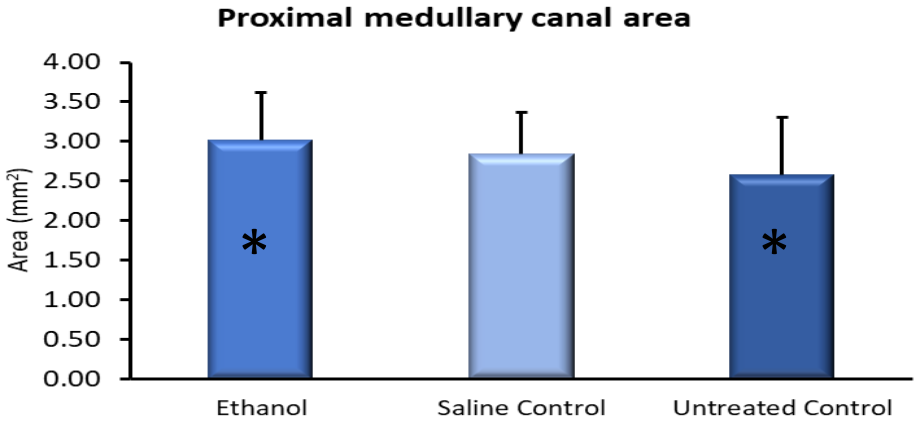

Figure 3.11: Proximal medullary canal area. The mean medullary area at the 25th percentile mark is given for the three groups studied. (Error bars represent standard deviation and stars indicate statistical significance).

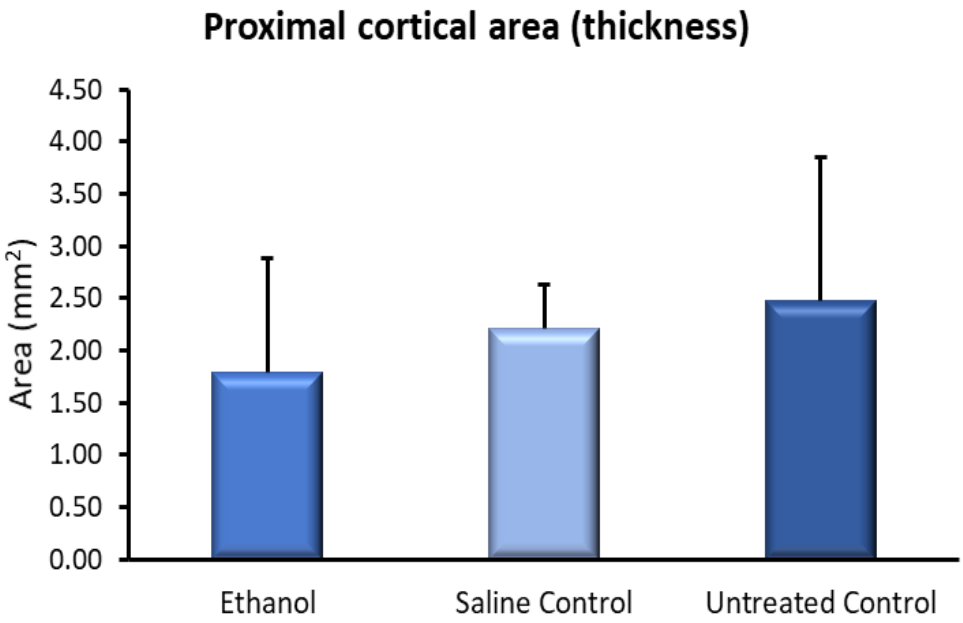

Figure 3.12: Proximal cortical area. The mean cortical area at the 25th percentile mark is given for the three groups studied. Error bars represent standard deviation.

Midshaft cross-sectional area, cortical area (thickness) and medullary canal area

The midshaft cross sectional area was similar in all three groups studied. The ethanol group had mean of 2.48 mm^2 ±0.41 and the saline and untreated groups had 2.51 mm^2 ±0.37 and 2.45 mm^2 ±0.44, respectively (Fig. 3.13). The medullary canal area was greater in the ethanol group (1.01 mm^2 ±0.25) in comparison to the saline and untreated controls (Mean=0.96 mm^2 ±0.16 and 0.86^2 mm^2 ±0.12 respectively). Significant differences in medullary canal area where observed between the ethanol and untreated controls (p=0.05) (Fig. 3.14). Regarding cortical area (thickness) in this bone region, the ethanol group (Mean=1.47 mm^2 ±0.32) exhibited a marginally lower value compared to the saline and untreated controls which had the same size area (Mean=1.5 mm^2 ±0.25 and ±0.45, respectively) (Fig. 3.15).

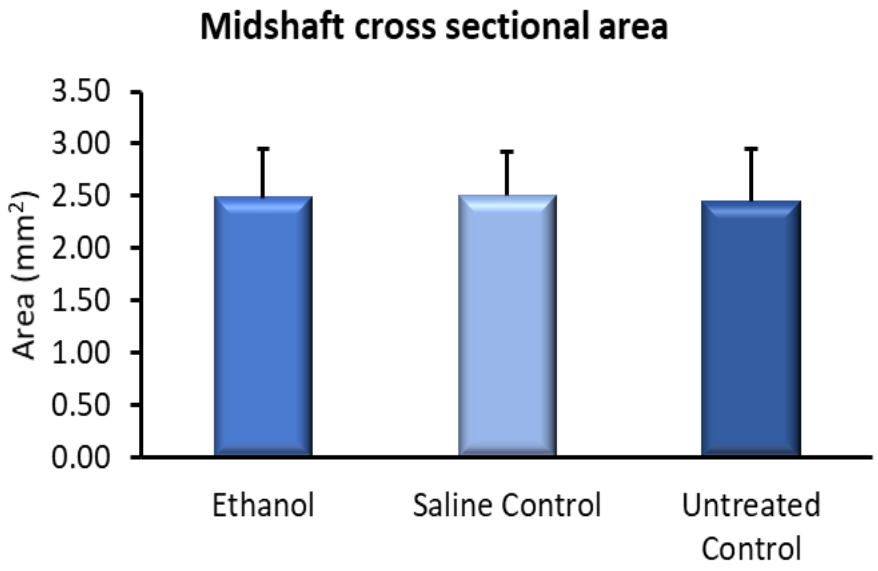

Figure 3.13: Midshaft cross-sectional area. The mean cortical area at the 50th percentile mark is given for the three groups studied. Error bars represent standard deviation.

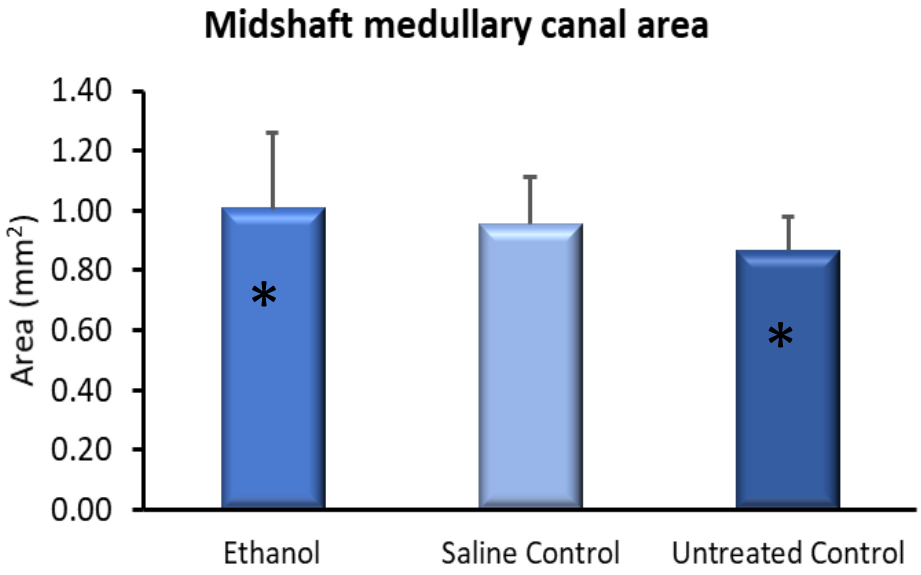

Figure 3.14: Midshaft medullary canal area. The mean medullary canal area at the 50th percentile mark is given for the three groups studied. (Error bars represent standard deviation and stars indicate statistical significance).

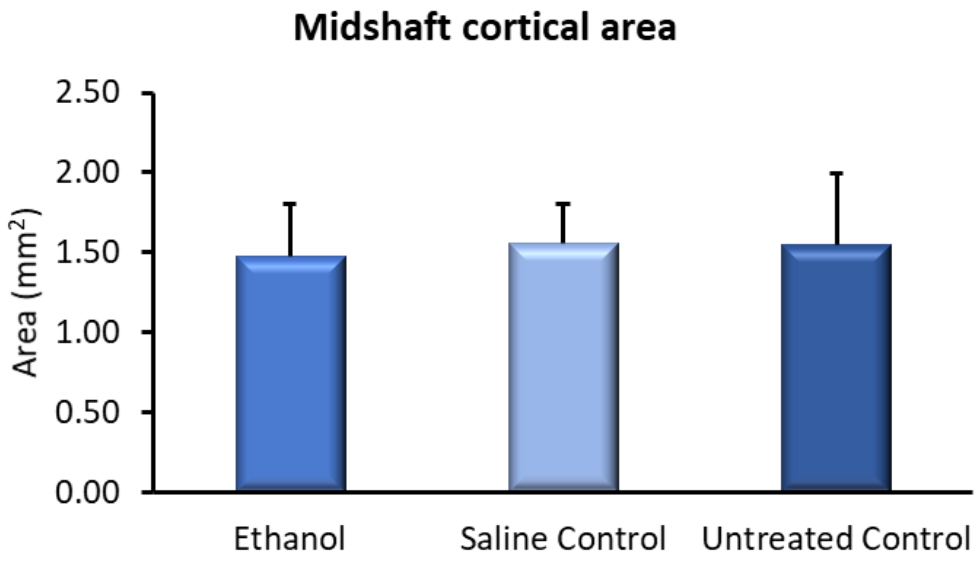

Figure 3.15: Midshaft cortical area. The mean medullary canal area at the 50th percentile mark is given for the three groups studied. Error bars represent standard deviation.

Relationship of cross sectional area with cortical thickness and medullary thickness

In the proximal region, the ethanol group cross sectional area was highly correlated with the medullary canal area (R=0.551, p=0.008) and cortical thickness (R=0.888, p=<0.001) (Table 3.2). This was also observed in the saline controls medullary canal area (R=0.956, p=<0.001) and cortical thickness (R=0.929, p=<0.001) (Table 3.2).

Similarly, in the midshaft, the ethanol group cross sectional area was highly correlated with the medullary canal area (R=0.612, p=0.002) and cortical thickness (R=0.784, p=<0.001) (Table 3.2). This pattern of high correlation also occurred in the saline group with the midshaft cross sectional area being correlated with the medullary canal area (R=0.849, p=<0.001) and cortical thickness (R=0.942, p=<0.001) (Table 3.2).

Table 3.2: Pearson's correlation of cross sectional area with cortical thickness and medullary thickness in the ethanol group and saline controls

		Ethanol		Saline Control	
		Medullary Canal Area	Cortical Thickness	Medullary Canal Area	Cortical Thickness
Proximal	Correlation	0.551	0.888	0.956	0.929
Cross Sectional	p value	0.008	<0.001	<0.001	<0.001
Area	N	22	22	24	24
Midshaft	Correlation	0.612	0.784	0.849	0.942
Cross Sectional	p value	0.002	<0.001	<0.001	<0.001
Area	N	22	22	21	21

Relationship of osteometric and trabecular morphometric parameters.

In the ethanol group, full bone length was highly correlated with shaft length (R=0.864, <0.001) and proximal volume (R=0.654, p=0.006) (Table 3.3). This high correlation of full bone length with shaft length (R=0788, <0.001) and proximal volume (R=0.649, p=0.001) was also observed in the saline control group (Table 3.4).

In the ethanol group, shaft length was correlated with proximal volume (R = 0.756, p =0.001) and negatively correlated with trabecular thickness (Tb.Th) (R=-0.540, p=0.031) (Table 3.3). In contrast, there was no correlation of either full bone or shaft length with trabecular properties in the saline control group (Table 3.4).

The ethanol group had a negative correlation of bone to total volume ratio (BV/TV) with trabecular number (TbN) (R=-0.508, p=0.016) and spacing (Tb.Sp) (R= -0.459, p=0.032). Trabecular thickness (Tb.Th) exhibited a negative correlation with trabecular number (TbN) (R=-0.442 p=0.04) in the ethanol group (Table 3.3). In the saline control

group, the proximal volume was negatively correlated with trabecular spacing (Tb.Sp) (R=-0.513, p=0.025). There was a negative correlation of bone to total volume ratio (BV/TV) with trabecular spacing (Tb.Sp) (R= -0.0659, p=0.002) (Table 3.4).

Table 3.3: Pearson's correlation of osteometric as well as trabecular morphometric parameters in the ethanol group (Significant values in red).

		Full Bone Length	Shaft Length	Proximal Volume	BV/TV Proximal	TbTh Proximal	TbN Proximal	TbSp Proximal
Full Bone Length	Correlation	1	0.864	0.654	0.422	-0.364	-0.458	-0.332
	P value		<0.001	0.006	0.104	0.165	0.075	0.208
	N	16	16	16	16	16	16	16
Shaft Length	Correlation	0.864	1	0.756	0.445	-0.540	-0.478	-0.366
	P value	0.000		0.001	0.084	0.031	0.061	0.163
	N	16	16	16	16	16	16	16
Proximal Volume	Correlation	0.654	.756	1	0.400	-0.285	-0.329	-0.297
	P value	0.006	0.001		0.124	0.285	0.214	0.263
	N	16	16	16	16	16	16	16
BV/TV Proximal	Correlation	0.422	0.445	0.400	1	0.338	-0.508	-.459
	P value	0.104	0.084	0.124		0.124	0.016	0.032
	N	16	16	16	22	22	22	22
TbTh Proximal	Correlation	-0.364	-0.540	-0.285	0.338	1	-0.442	0.229
	P value	0.165	0.031	0.285	0.124		0.040	0.305
	N	16	16	16	22	22	22	22
TbN Proximal	Correlation	-0.458	-0.478	-0.329	-0.508	-0.442	1	-.424
	P value	0.075	0.061	0.214	0.016	0.040		0.050
	N	16	16	16	22	22	22	22
TbSp Proximal	Correlation	-0.332	-0.366	-0.297	-0.459	0.229	-0.424	1
	P value	0.208	0.163	0.263	0.032	0.305	0.050	
	N	16	16	16	22	22	22	22

Table 3.4: Pearson's correlation of osteometric and trabecular morphometric parameters in the saline controls (significant values in red).

		Full Bone Length	Shaft Length	Proximal Volume	BV/TV Proximal	TbTh Proximal	TbN Proximal	TbSp Proximal
Full Bone Length	Correlation	1	0.788	0.649	-0.360	-0.449	0.167	0.041
	P value		<0.001	0.001	0.130	0.054	0.494	0.868
	N	22	22	22	19	19	19	19
Shaft Length	Correlation	0.788	1	0.392	-0.381	-0.423	-0.122	0.271
	P value	<0.001		0.071	0.107	0.071	0.619	0.262
	N	22	24	22	19	19	19	19
Proximal Volume	Correlation	0.649	0.392	1	0.268	-0.147	0.244	-0.513
	P value	0.001	0.071		0.268	0.547	0.315	0.025
	N	22	22	22	19	19	19	19
BV/TV Proximal	Correlation	-0.360	-0.381	0.268	1	0.357	0.138	-0.659
	P value	0.130	0.107	0.268		0.133	0.573	0.002
	N	19	19	19	19	19	19	19
TbTh Proximal	Correlation	-0.449	-0.423	-0.147	0.357	1	-0.364	-0.208
	P value	0.054	0.071	0.547	0.133		0.125	0.393
	N	19	19	19	19	19	19	19
TbN Proximal	Correlation	0.167	-0.122	0.244	0.138	-0.364	1	-0.094
	P value	0.494	0.619	0.315	0.573	0.125		0.702
	N	19	19	19	19	19	19	19
TbSp Proximal	Correlation	0.041	0.271	-0.513	-0.659	-0.208	-0.094	1
	P value	0.868	0.262	0.025	0.002	0.393	0.702	
	N	19	19	19	19	19	19	19

Prediction of group membership using the cortical and medullary canal areas

A binary logistic regression analysis was conducted to predict membership to the ethanol or saline control group using, cortical area (thickness) and medullary canal area as predicting variables. A test of the full model against a constant only model was statistically significant, indicating that the predictors as a set reliably distinguished between ethanol and saline control group membership (Chi square = 17.608, p = 0.007 with df = 6). Nagelkerke's R^2 of 0.487 indicated a moderately strong relationship between prediction and grouping. The Wald criterion demonstrated that only proximal medullary canal area made a significant contribution to prediction of group membership (p=0.02) (Table 3.5). Prediction success overall was 74.4% (72.7% for the ethanol group and 76.2% saline controls (Table 3.6).

Table 3.5: Cortical and medullary canal area variables in the equation

Variables in the Equation

	B	S.E.	Wald	df	Sig.	Exp(B)
Proximal Medullary Area	-3.882	1.67	5.4	1	0.02	0.021
Proximal Cortical Thickness	2.008	1.623	1.531	1	0.216	7.449
Midshaft Medullary Area	0.219	2.774	0.006	1	0.937	1.244
Midshaft Cortical Thickness	3.955	3.691	1.148	1	0.284	52.196
Constant	-0.422	2.608	0.026	1	0.872	0.656

Table 3.6: Group membership classification from cortical and medullary canal area variables.

Classification Table

Observed		Predicted		
		Group		Percentage Correct
		Ethanol	Saline Control	
Group	Ethanol	16	6	72.7
	Saline Control	5	16	76.2
Overall Percentage				74.4

Prediction of group membership using the trabecular morphometric parameters

A binary logistic regression analysis was conducted to predict membership to either the ethanol or saline control group using bone volume to total volume ratio, trabecular thickness, number and separation as predicting variables. A test of the full model against a constant only model was statistically significant, indicating that the predictors as a set reliably distinguished between ethanol or saline control group membership (Chi square = 16.995, $p < 0.002$ with df = 4). Nagelkerke's R^2 of 0.453 indicated a moderately strong relationship between prediction and grouping. The Wald criterion demonstrated that no particular parameter solely made a significant contribution to prediction of group membership as all the parameters did not show significance (Table 3.7). Prediction success overall was 68.3% (81.8% for the ethanol group and 52.6% in saline controls (Table 3.8).

Table 3.7: Trabecular morphometric parameters in the equation

Variables in the Equation

	B	S.E.	Wald	df	Sig.	Exp(B)
BV/TV Proximal	10.156	7.574	1.798	1	0.18	25747.087
TbTh Proximal	16.476	11.574	2.026	1	0.155	14301840.51
TbN Proximal	1.214	0.715	2.881	1	0.09	3.367
TbSp Proximal	32.783	22.344	2.153	1	0.142	172811444
Constant	-16.975	8.935	3.61	1	0.057	0

Table 3.8: Group membership classification from trabecular morphometric parameters.

Classification Table

Observed		Predicted		
		Group		Percentage Correct
		Ethanol	Saline Control	
Group	Ethanol	18	4	81.8
	Saline Control	9	10	52.6
Overall Percentage				68.3

Parameters accounting for the ethanol group

Principal components analysis with varimax rotation was conducted to assess how six bone morphology parameters clustered. These variables were bone length, proximal volume, BV/TV, Tb.Th, TbN, TbSp. The assumption of independent sampling was met as the KMO test (0.616) exhibited that enough items were predicted by each factor (Table 3.9). The variables are correlated highly enough to provide a reasonable basis for principal component analysis as shown by the Bartlett test (p=0.005) (Table 3.10). Two components were rotated, based on the eigenvalues above 1 criterion. After rotation,

the first component accounted for 35.28% of the variance, and the second component accounted for 33.66% of the variance. The ratio of bone volume to total volume (BV/TV) and TbN were the main factors in component one (loading above ±9). Bone length, proximal volume and Tb.Th were the major factors in component two (Table 3.11). Both these first two components together accounted for 68.94% of the outcome. Other factors not in this model may have accounted for the remaining percentage. Trabecular number (TbN), thickness (TbTh) and spacing (TbSp) had an inverse relationship with other parameters, and as such where clustered separately as shown by the rotated space component plot (Table 3.11 and Fig. 3.12).

Table 3.9: Kaiser-Meyer-Olkin (KMO) Measure of Sampling Adequacy and Bartlett's Test in the ethanol group

KMO and Bartlett's Test

Kaiser-Meyer-Olkin Measure of Sampling Adequacy.		0.616
Bartlett's Test of Sphericity	Approx. Chi-Square	32.569
	df	15
	Sig.	0.005

Table 3.10 Total variance explained by each component in the ethanol group. Eigenvalues as well as the loadings of each component is given based on Eigenvalues of one or above.

Total Variance Explained

Component	Initial Eigenvalues			Rotation Sums of Squared Loadings		
	Total	% of Variance	Cumulative %	Total	% of Variance	Cumulative %
1	2.718	45.296	45.296	2.117	35.28	35.28
2	1.419	23.644	68.94	2.02	33.66	68.94
3	0.9	15.003	83.943			
4	0.524	8.726	92.668			
5	0.323	5.376	98.044			
6	0.117	1.956	100			

Table 3.11: Rotated Component Matrix in the ethanol group. The Varimax rotation method with Kaiser normalization was used.

Rotated Component Matrix

	Component	
	1	2
BV/TV Proximal	**0.941**	0.152
TbN Proximal	**-0.912**	-0.156
Bone Length	**0.386**	**0.793**
Proximal Volume	**0.336**	**0.754**
TbTh Proximal	**0.351**	**-0.726**
TbSp Proximal	-0.116	**-0.498**

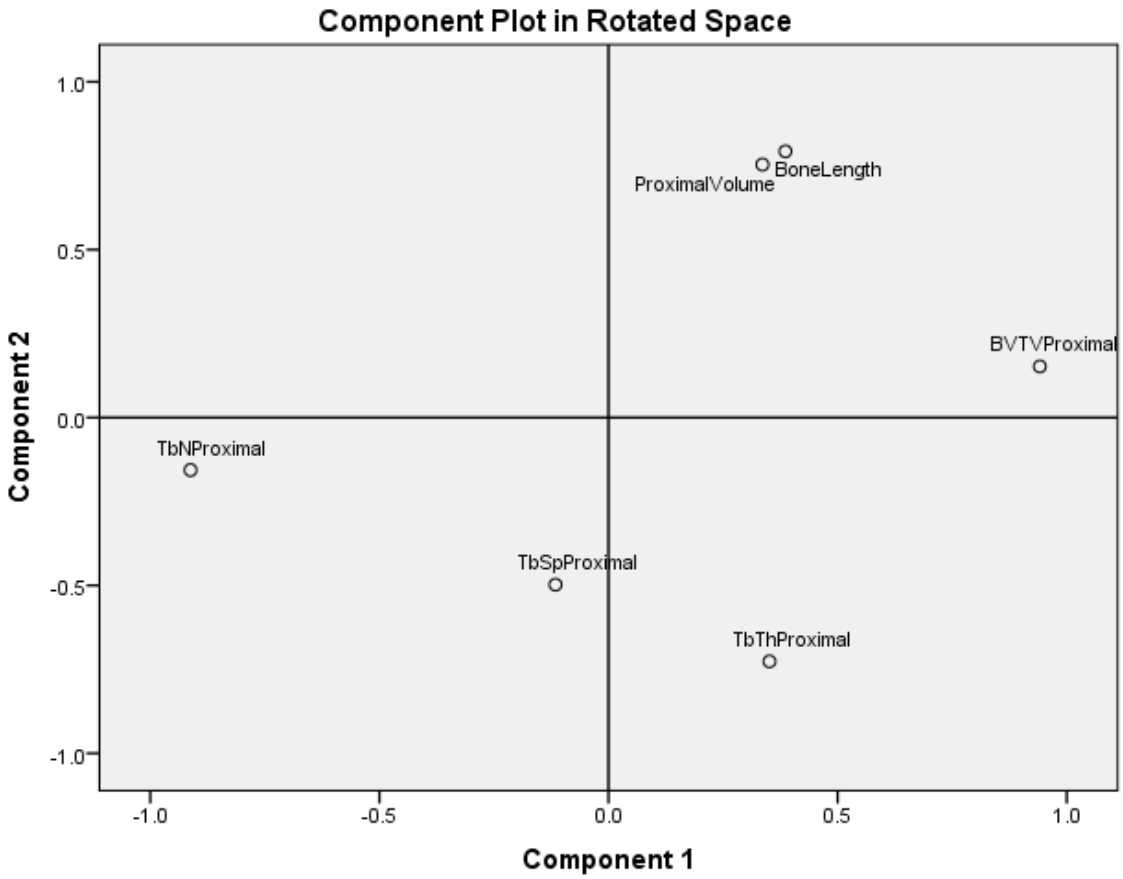

Figure 3.16: Graphical representation of how the variables clustered in the ethanol group.

Parameters accounting for the saline control group

Principal components analysis with varimax rotation was conducted to assess how six bone morphology parameters clustered. These variables were bone length, proximal volume, BV/TV, Tb.Th, TbN, TbSp. The assumption of independent sampling was met as the KMO test (0.538) exhibited that enough items were predicted by each factor (Table 3.12). The variables are correlated highly enough to provide a reasonable basis for principal component analysis as shown by the Bartlett test (p=0.005) (Table 3.12). Two

components were rotated, based on the eigenvalues above 1 criterion. After rotation, the first component accounted for 34.627% of the variance, and the second component accounted for 34.447% of the variance. The ratio of bone volume to total volume (BV/TV) and TbN were the main factors in component one (loading above ±9). Bone length, proximal volume and Tb.Th where the major factors in component two (Table 3.13). Both these first two components together accounted for 69.074% of the outcome. Other factors not in this model may have accounted for the remaining percentage.

Trabecular number (TbN) and thickness (TbTh) had an inverse relationship with other parameters, and as such where clustered separately as shown by the rotated space component plot (Table 3.14 and Fig. 3.16).

Table 3.12 Kaiser-Meyer-Olkin (KMO) Measure of Sampling Adequacy and Bartlett's Test in the saline control group

KMO and Bartlett's Test

Kaiser-Meyer-Olkin Measure of Sampling Adequacy.		0.538
Bartlett's Test of Sphericity	Approx. Chi-Square	40.562
	df	15
	Sig.	0.000

Table 3.13 Total Variance Explained by each component in the saline controls. The Eigenvalues as well as the loadings of each component is given based on Eigenvalues of one or above.

Total Variance Explained

Component	Initial Eigenvalues			Rotation Sums of Squared Loadings		
	Total	% of Variance	Cumulative %	Total	% of Variance	Cumulative %
1	2.079	34.643	34.643	2.078	34.627	34.627
2	2.066	34.431	69.074	2.067	34.447	69.074
3	0.995	16.58	85.655			
4	0.465	7.748	93.403			
5	0.265	4.411	97.814			
6	0.131	2.186	100			

Table 3.14: Rotated components using the Varimax with Kaiser Normalization in the saline controls.

Rotated Component Matrix

	Component	
	1	2
BV/TV Proximal	**0.892**	-0.153
TbSp Proximal	**-0.887**	-0.156
Bone Length	-0.195	**0.854**
Proximal Volume	0.502	**0.756**
TbTh Proximal	**0.433**	**-0.663**
TbN Proximal	0.130	**0.527**

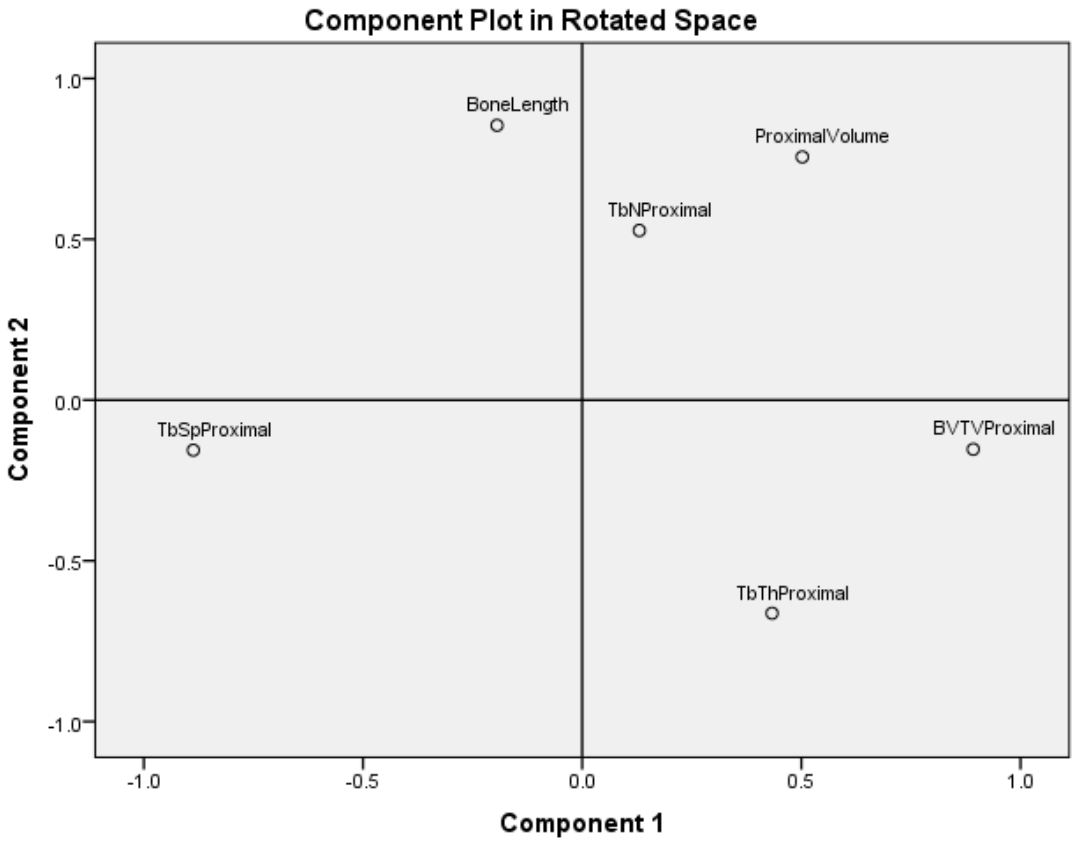

Figure 3.17: Graphical representation of how the variables in the saline group are clustered in a three-dimensional space

CHAPTER 4: DISCUSSION

The current study employed histological, immunohistological and micro focus X-Ray computed tomography to understand how prenatal alcohol exposure affects bone development in the *Sprague-Dawley* rat tibia. We studied the proximal tibial growth plate to evaluate the observation that prenatal alcohol consumption results in diminished stature of the offspring (Chakkalakal et al., 2002; Keiver and Weinberg, 2004; Ramadoss et al., 2006). This involved histomorphometric analysis of chondrocyte number, proliferative and hypertrophic zone length, as well as growth plate area. We proposed that reduced cell proliferation could contribute to the observed smaller stature in prenatal alcohol consumption. We tested the validity of this theory by immunolabelling proliferating chondrocytes in the epiphyseal growth plate with the Ki-67 antibody. Osteometric dimensions of the tibia were included to gain an estimation of bone size. The proximal part of the tibia was studied to understand how weak bones and osteoporosis may occur (Turner et al., 2001; Simpson et al., 2005; Maddalozzo et al., 2009). This involved use of Micro CT to quantify trabecular, thickness, number, separation and estimation of bone volume.

4.1 Rat model of fetal alcohol syndrome

In the current study, a model of moderate binge drinking was utilized. This model is appropriate in the South African context as reports exist in the literature showing that some women tend to take massive amounts of alcohol within a short duration (binge drinking) (Conover and Jones, 2012). This is due to the stigma associated with alcohol consumption by females in certain communities. The high level of basic health illiteracy

also contributes to alcohol intake during pregnancy although many women stop drinking once they know that they are pregnant.

We used three groups; ethanol treated, saline controls and untreated controls. The later was to control for the potential effects of stress as treatment was through oral gavage, which may elevate stress levels and possibly affect pregnancy. The pregnant rats received a daily single dose of ethanol to mimic regular binge drinking. As alcohol has more calories than rat feed, we expected the ethanol treated animals to either gain more weight than controls or to consume less food or both. However, we found that weight gain and food consumption were similar in all three study groups.

While the blood alcohol was elevated as measured an hour following treatment, a major concern was that rats metabolize alcohol faster than humans as the peak blood ethanol concentration in rodents occurs an hour after administration. Normal blood alcohol levels in rats are exhibited two hours after treatment (Snow and Keiver, 2007). Since only a single ethanol dose was given per day, this effectively means that the fetus would be exposed to alcohol for a limited time (approximately 2 hours) daily. This could potentially impact on the ability to induce gestational alcohol exposure effects.

We chose a dose of 25.2% ethanol in light of the fact that a lower dose could potentially fail to induce the intended effect on the offspring. A higher dose could increase the risk of failed implantations and spontaneous abortions. Reports suggest that prenatal alcohol may result in stillbirths, self-abortion and resorption, and this may results in fewer pups being born in the ethanol group (Simpson et al., 2005; Snow and Keiver, 2007). In the present study, there were no significant differences in litter size

and gestation duration although the ethanol group had fewer pups. This suggests that the dose and frequency of ethanol administration employed in this study does not affect gestation duration and liter size based on the non-statistical significance observed among the groups.

4.2 Prenatal alcohol exposure effects on proximal tibia growth plate

Growth plate size

Alcohol has been shown to cause changes in the growth plate resulting in a delay in bone development (Miralles-Flores and Delgado-Baeza, 1992). In agreement with this, the growth plate exhibited a smaller surface area in comparison with the controls in the present study with significant differences between the experimental group and the untreated group.

Proliferative zone surface area and cell count

In the proliferative zone of the growth plate, we found both fewer cells and a smaller surface area in the ethanol treated groups compared to the saline and untreated controls. As the epiphyseal plate is responsible for longitudinal growth (Nilsson and Baron, 2004; Lui et al., 2011), this could be one of the reasons for the shorter stature exhibited by FAS children. Miralles-Flores and Delgado-Baeza (1992) investigated the effects of gestational alcohol exposure administering 36% ethanol on 0 and 15 day postnatal pups. Changes in the epiphyseal plate were only shown on the later but not on the former. However, Snow and Keiver (2007) found that gestational alcohol affected pups that were surgically removed at 21 days of gestation.

Using the anti-KI-67 antibody to label proliferating cells, the ethanol group exhibited fewer proliferating cells. The mechanisms in which alcohol affects the proliferative zone are unknown. It is possible that alcohol disturbs cell chondrocyte proliferation in one or more of the cell division phases, resulting in slow proliferation rate. Another possibility is induction of apoptosis, due to a potential DNA damage caused by the teratogenic effects of alcohol. Moreover this study produced large differences in the standard deviations with regards to ki-67 positive cells in the untreated group, which may be due to differences in sex with in the group. Further studies are required to ascertain these theories.

Hypertrophic zone surface area and cell count

The hypertrophic zone comprises chondrocytes that are older and larger than the chondrocytes found in the proliferative zone. The more mature cells are located closer to the diaphyseal end of the plate. In the hypertrophic zone, lipids, glycogen, and alkaline phosphatase accumulate, resulting in the calcification of the cartilaginous matrix. The longitudinal growth of bone is a result of cellular division in the proliferative zone along with the maturation of cells in the hypertrophic zone. The ethanol group had less number of cells and the surface area of the hypertrophic zone was reduced in comparison to the control groups. This was similar to the findings of Miralles-Flores and Delgado-Baeza (1992). However, this contrasts the findings by Snow and Keiver (2007), which showed an increase in the surface area of the hypertrophic zone. The difference between these two are that in the Miralles-Flores and Delgado-Baeza (1992) study, dams were given alcohol for 30 days prior to and

during gestation (3 weeks), while in the study of Snow and Keiver (2007) the dams were fed ethanol 3 weeks prior and 3 weeks during gestation. The differences reported may also have been due to differences in the ages of the rats, since the regulation of bone development varies between pre and postnatal development. Likewise, this may be attributed to the effect of in utero ethanol exposure on the expression of local growth factors and systemic hormones which affect osseous tissue development differently during pre and postnatal periods. Furthermore, differences between the duration of alcohol exposure in the studies may account for the differences reported in the hypertrophic zone. It is clear that research in this area is limited, with only few studies focusing on the effects of prenatal alcohol on longitudinal growth. Growth retardation is one of the main characteristics of FAS; insight into how the epiphyseal plate is affected by gestational alcohol could provide valuable information in paving the way for appropriate treatment regimens to combat this devastating impact on growth.

4.3 Osteometric and bone internal morphology

Bone length

The full and shaft length of the tibia was similar among all three groups in the study. In contrast, previous studies found shorter tibiae in the ethanol group (Miralles-Flores and Delgado-Baeza, 1992; Simpson et al., 2005; Snow and Keiver, 2007). In the present study, we used 25.2% ethanol whereas other researchers used a higher ethanol concentration of 36% studies (Miralles-Flores and Delgado-Baeza, 1992; Simpson et al., 2005; Snow and Keiver, 2007). The effects of prenatal ethanol exposure on bone are dose dependent as (Simpson et al., 2005; Snow and Keiver, 2007; Turner et al., 2012)

showed that 36% ethanol causes more adverse effects than 25% and 15% ethanol administered in gestation. A possibility exists that we could have found a shorter length had we used a higher concentration such as 36%.

Also our results could be attributed to the ages of the rat pups used, our study reported on the tibial length of postnatal 3 week old pups in comparison to previous reports, in these studies the rat pups were aged 21 day gestation and 0 as well as 15 day postnatal, respectively (Miralles-Flores and Delgado-Baeza, 1992; Snow and Keiver, 2007).

The gestation duration in our study could have contributed to the similar bone lengths we observed as we allowed the dams to give birth naturally resulting in a gestation range of 19-24 days. However, there was no statistical significance in gestation duration in our study. Other researchers controlled for variation in gestation duration by surgically removing the pups at 21 days gestation. Since treatment was stopped at gestation day 19, some liters may have had a intrauterine recovery period between end of treatment and term (birth) (Miralles-Flores and Delgado-Baeza, 1992; Simpson et al., 2005; Snow and Keiver, 2007).

Considering the relatively high rate of alcohol metabolism in rats, these animals in our study were only exposed to ethanol for approximately 2 hours per day as that is the time it takes for rodents to metabolise ethanol (Simpson et al., 2005; Snow and Keiver, 2007). This, combined with the moderate dose of 25.2% ethanol could have protected the rats from the effects of alcohol.

These results could potentially be different in humans as most people who drink during pregnancy are less educated and also have lower socioeconomic status, which impacts their diet (May et al., 2013). As the animals were on a nutritious balanced diet, this could have mitigated the effects of ethanol. Additionally, there was a 3-week postnatal period of no ethanol exposure which may have improved the chances of recovery in some respects such as bone length. Spohr et al. (1993) and (Streissguth et al., 1991) suggested that that there is potential for catch up growth following prenatal exposure to ethanol. This proposition requires further studies to establish the facts.

Trabecular bone

In the present study, we found both bone volume to total volume (BV/TV) and trabecular thickness (TbTh) to be lower in the ethanol group in comparison with the controls. This finding is similar to previous reports using growing rats (Sampson et al., 1996; Sampson et al., 1997a) and in adult rats (Diamond et al., 1989; Wezeman et al., 1999; Turner et al., 2001; Maddalozzo et al., 2009) who showed that alcohol intake reduces trabecular bone volume and aids trabecular thinning. Children with FAS have a higher risk of osteoporosis (Jones and Dwyer, 2000). Osteoporosis is a skeletal disease, characterized by reduction in bone mass and disruption of trabecular and compact bone structure, resulting in a loss of mechanical strength and an increased fracture risk (Soares et al., 2010). These features are observed in alcohol fed rats (Hogan et al., 1997; Wezeman et al., 1999; Mikosch, 2014) and in young, growing rats (Sampson et al., 1996). Similarly, Chen et al. (2001) found a decrease in trabecular number in the hamster femur following alcohol consumption. This is thought to be due to a decrease

in the osteoblast number and size as previously reported in alcohol exposed rats (Diez et al., 1997).

Having not seen differences in bone length among the three groups, we queried whether a size estimation method that includes more dimensions would yield the same observations. Linear measurements such as length are in a single dimension and as such tend to miss size information from other dimensions in three-dimensional space. We then, calculated the proximal volume (part below the growth plate) as this is the portion rich in trabeculae. We found that the proximal volume was significantly less in the ethanol group compared to the controls despite similar bone lengths. This finding suggests that alcohol affects the proximal volume

The trabecular number (TbN) was not affected in our study. This is similar to the findings by, who did not find any changes on the TbN in the proximal tibial epiphysis. However, there was more trabecular spacing in the ethanol group. This considered together with the lower BV/TV, TbTh and TbSp suggests that, although the bone length was similar in all groups, the internal morphology was not the same among the study groups. This means that prenatal alcohol exposure may affect internal architecture while sparing the external bone length. This disruption of the internal bone morphology may also explain why FAS children are prone to osteoporosis and fracture as they may have less bony material internally. Furthermore the present study produced large standard deviations in relation to trabecular thickness and spacing in the untreated group. This is possibly due to the differences between male and female rats as this was not accounted for.

4.4 Parameters most affected by prenatal ethanol exposure

Employing a binary logistic regression it was found that the proximal medullary canal area was the main parameter that determined group membership into either ethanol treated or saline control. This means that the proximal medullary canal area is one of the most affected variables in gestational alcohol exposure.

Our study found of a positive correlation between medullary canal area and cortical thickness. This indicates that the smaller medullary canal was coupled with thinner cortical bone. We propose that this may potentially explain weaker bones observed in FAS children.

The negative correlation of BV/TV with trabecular number and spacing in the ethanol group indicates that when there was more bone, there was less trabecular and with smaller spaces in between. This means that in the ethanol group, there may have been a delay in trabecular formation.

Principal Component Analysis (PCA) showed that the proximal volume, ratio of bone volume to total volume (BV/TV), trabecular thickness (TbTh), trabecular number (TbN) and trabecular spacing (TbSp) were the main components in both the ethanol and saline controls. In the ethanol group, TbTh, TbSp and TbN had negative loadings to the PCA model. These two parameters were also negatively correlated. This further supports our suggestion that trabecular formation may have been delayed in the ethanol group.

CHAPTER 5: CONCLUSIONS

Gestational alcohol exposure in the present study did not result in any gross anatomical abnormalities but had adverse effect on the growth plate with respect to its general size, respective zone sizes and the number of cells in each zone. This may be how diminished stature of the offspring occurs. Fewer proliferative cells were found using the anti-Ki67 antibody, indicating that in utero alcohol exposure slows cell proliferation, contributing to the small stature.

Logistic regression showed that the proximal medullary canal area and trabecular separation were the main parameters affected the most in gestational alcohol. The negative correlation of trabecular thickness and spacing in the ethanol group may be a contributor to bone weakness. These findings add new knowledge to how *in utero* alcohol affects the offspring.

5.1 Limitations

The limitations of this study include treatment administration, because of its stressful nature to the rats it was stopped on the 19th day of gestation. Hence the dams had 2-3 days without treatment during gestation, which could have then resulted in the reversal of the effects caused by the treatment.

5.2 Recommendations

Further studies employing different modes of treatment ensuring maximal exposure to alcohol might provide a comprehensible view of the effect of prenatal alcohol exposure on the postnatal development of bone. Additionally, the investigation of cell apoptosis

and growth factors, could lend an unambiguous understanding on the effects of gestational alcohol exposure on the biology of chondrocytes responsible for bone development.

APPENDICES

Appendix 1: Reagents used

- Chloroform (CAS NO. 67-66-3, Associated Chemical Enterprise, Johannesburg, RSA
- Citric Acid (19150 41, Riedel-de Haën AG, Germany)
- Mayer's solution (SAAR2422001LC, Merck Chemicals (Pty.) Ltd., Gauteng, RSA)
- Eosin yellowish (SAAR2186000DC, Merck Chemicals (Pty.) Ltd., Gauteng, RSA)
- Formaldehyde (Associated Chemicals Enterprise, Johannesburg, RSA)
- Nuclear fast red (Art No. 5189, Merck RGaA, Darmstadt, Germany)
- Xylene (CAS NO. 108-38-3, Associated Chemicals Enterprise, Johannesburg, RSA)
- Acetic acid (glacial) (Saarchem 1021020LC, Wadeville, Gauteng, RSA)
- Entellen (HX 088232, Merck RGaA, Darmstadt, Germany)
- Ferric chloride (SAAR2340530EM, Merck Chemicals (Pty.) Ltd., Gauteng, RSA)
- Basic fuschin (SAAR2501500DC), Merck Chemicals (Pty.) Ltd., Gauteng, RSA)
- Hydrochloric acid 1% (HCl) (Associated Chemicals Enterprise, Johannesburg, RSA)
- Tween 20 (616-45-00KF, Saarchem, Wadeville, Gauteng, RSA)
- Rabbit Specific HPR/DAB (ABC) detection IHC kit (ab624621 Abcam)
- Hydrogen peroxide (Catalog. 1037024, Merck (Pty.) Ltd., Gauteng, RSA)
- Potassium dihydrogen orthophosphate (CAS NO. 7778-77-0, Associated Chemicals Enterprise, Johannesburg, RSA)
- Potassium chloride (CAS NO. 7447-40-7, Associated Chemicals Enterprise, Johannesburg, RSA)
- Disodium hydrogen orthophosphate anhydrate (CAS NO. 7558-79-4, Associated Chemicals Enterprise, Johannesburg, RSA)
- Sodium chloride (CAS NO. 7647-14-5, Associated Chemical Enterprise, Johannesburg, RSA)

- Sodium hydrogen carbonate (CAS NO. 582-28-20, Saarchem (Pty.) Ltd., Krugersdorp, RSA)
- Sodium Iodate (The lab Depot, Inc)
- Potassium Alum (CAS NO. 7784-24-9, Associated Chemical Enterprises)
- 3-Aminoprpyl triethoxy silane (1010666628, Sigma Aldrich, Steinheim, Germany)
- Acetone (SAAR1022040LC, Merck Chemicals (Pty.) Ltd., Gauteng, RSA)
- Ammonium Oxalate (Catalog no. 1046946, Merck Chemicals (Pty.) Ltd., Gauteng, RSA)
- Formic acid (Catalog no. 1041684), Merck Chemicals (Pty) Ltd., Gauteng, RSA)
- Wax (Merck Chemicals (Pty.) Ltd., Gauteng, RSA)

Appendix 2: Equipment

- Automatic tissue processor (Shandon, Citadel 1000)
- Cassettes (Merck Chemicals (Pty.) Ltd., Gauteng, RSA)
- Ethanol Colorimetric Assay Kit (BioVision incorporation, Milpitas, USA)
- Embedding table (Miles Scientific, serial number 31602-554)
- Weighing scales:

  (Model- KERN EW600-2M, Ser. No. 8423167, Albstadt, Germany)

  (Model- SARTORIUS GMBH, Fabr. No. 36020123)

  (Snowrex electronic scale, Clover scales (Pty) Ltd, Model- WP 003)
- Incubator (Model-508-2U, Labcon shaker)
- Microhaematocrit centrifuge (Haematokrit 210, SN 0031 386-04, Hettich, Germany)
- iMark Bio-rad Microplate Absorbance Reader (Bio-rad Laboratories Inc, USA. Catalog number 168-1130)
- Digital Vernier caliper (series 530)
- Water bath (Model number 416, serial number SE 9455)
- ESCO Laboratory fume hood (Model: EFA-4UDW-8. Serial: 2011-60070
- Microtome (Leica RM 2125RM, Fabr. Nr. 07390329)
- Microscope (axioscope) (Model Axiocom HRC, identification number 105-041756)
- Microfocus computed tomography (µCT) X-ray machine (NIKON XTH 225/320 LC)
- Microscope Slides (3000F-02-1009, Lasec, Gauteng, RSA)
- Moulds (Merck Chemicals (Pty.) Ltd., Gauteng, RSA)

Appendix 3: Software packages

- Microsoft Excel 2016 (Microsoft Corporation)
- SPSS version 24
- Volume Graphics Studio (VGS) software
- Axiovision (AXIOVs) version 4.7.2.0 (Carl Zeiss microscopy)
- Fiji Image-J software

Appendix 4: Preparation of 10% neutral buffered formalin (10%NBF)

For 1000mls

1. Measure 900mls of distilled water
2. Add 9g of NaCl
3. Add 12g of Na_2HPO_4
4. Place in a beaker and stir using magnetic stirrer until clear
5. Add 100ml of formalin
6. Store at room temperature

Appendix 5: Determination of blood ethanol concentration

1. Dilute samples with assay buffer (1:10 dilution) in a clean test tubes.
2. Prepare Reaction Mix (46µl Ethanol assay buffer, 2µl Ethanol probe, and 2µl Ethanol Enzyme Mix)
3. Add 50µl of the Reaction Mix to all the test tubes
4. Incubate for 60 minutes at room temperature in a dark environment.
5. Measure O.D. 570nm
6. Correct background (difference of background value derived from the ethanol control from all the samples)
7. Calculate ethanol concentration from the standard curve, multiplied by the dilution factor.

   C = Sa/Sv nmol/µl or mM

   Where: **Sa** = sample amount from the Standard Curve (nmol)

   Sv = sample volume added into the samples (µl)

   Ethanol molecular weight: 46.07g/mol

Appendix 6: Tissue decalcification

Methods

1. Put tissue samples in cassettes and immerse in slowly running tap water for 30 minutes
2. Put tissue samples in EDTA for 3 weeks
3. Put tissue sections in running tap water for 30 minutes

Appendix 7: Decalcification end point

Methods

1 Take 5mls of EDTA in to separate test tube

2. Add 10mls ammonium oxalate
3. Mix well and allow to stand overnight
4. Examine for precipitate
5. Repeat if there is precipitate, until no precipitate forms and the solution is clear
6. Rinse in running tap water if no precipitate

Appendix 8: Tissue Processing

The tissue was processed using an automatic tissue processor (Shandon citadel 1000) as follows:

1. 10% buffered formalin for 4 hours
2. 70% alcohol for 1 hour
3. 95% alcohol for 2 hours
4. 95% alcohol for 2 hours
5. 95% alcohol for 2 hours
6. 95% alcohol for 2 hours
7. 100% alcohol for 2 hours
8. 100% alcohol for 2 hours
9. 100% alcohol for 2 hours
10. Chloroform for 2 hours
11. Chloroform for 2 hours
12. Wax for 2 hours
13. Wax for 2 hours

Appendix 9: Paraffin embedding

1. Warm the wax as well as the metal moulds and a pair of forceps making sure that the temperature does not exceed 60°C.
2. Once the wax has melted, fill the metal mould with wax.
3. Using the warmed forcep, gently orient the specimens such that the anterior surface of the proximal end faces the floor of the mould.
4. Cool briefly, and then cover with the plastic cassette accordingly.
5. Quickly top up with more melted wax and cool for approximately 20 minutes.
6. Separate the metal mould from the plastic cassette.

Appendix 10: Silane coated slides

APES solution

1. 3-Aminopropytriethoxysilane 4mls
2. Acetone 200mls

Methods

1. Immerse slides in APES solution
2. Rinse 2x in acetone for 10 dips
3. Rinse 2x in distilled water for 10 dips
4. Air dry at angle of 45^0
5. Incubate at 37^0 overnight

Appendix 11: Staining of tissue sections

Appendix 11.1: Mayer's Haematoxylin and eosin staining

Haematoxylin solution

For 1000mls

1. Haematoxylin 1g
2. Aluminium potassium sulphate (Potassium alum) 50g
3. Sodium iodate 0.2g
4. Citric acid 1g
5. Chlorate hydrate 50g
6. Allow haematoxylin, alum and sodium iodate to dissolve overnight.
7. Add chloral hydrate and citric acid
8. Boil solution for 5 minutes and then allow to cool.

Eosin solution

For 1000mls

1. Measure 1000mls of distilled water
2. Add 8g of stock eosin
3. Add 2g of erythron
4. Stir using a magnetic stirrer

Methods

Hydration

1. Dewax in xylene for 2x10 minutes.
2. Immerse in 2 changes of 100% ethanol for 3 minutes each
3. Immerse in 95% ethanol for 3 minutes
4. Immerse in 70% ethanol for 3 minutes
5. Wash in distilled water for 5 minutes

Nuclear staining

1. Stain with Mayer's haematoxylin for 10 minutes

2. Wash in running tap water for 2 minutes
3. Differentiate in 1% acid alcohol for 2 dips
4. Wash in running tap water for 2 minutes
5. Blue in Scott's tap water for 2 minutes
6. Wash in running tap water for 2 minutes

Cytoplasm staining

1. Stain in eosin for 2 minutes
2. Wash briefly in running tap water

Dehydration and mounting

1. Immerse in 70% ethanol for 3 minutes
2. Immerse in 90% ethanol for 10 minutes
3. Immerse in 100% ethanol for 10 minutes
4. Clear in 2 changes of xylene
5. Mount in entellen

Results

Nuclei: Blue-black

Muscle fibers: deep pinky red

Cytoplasm: Varying shades of pink.

Appendix 11.2: Scott's tap water solutions

For 100mls

1. Sodium hydrogen carbonate	2g
2. Magnesium sulphate	20g
3. Distilled water	1000ml

Dissolve the salts in the water and store in stock solutions at room temperature.

Appendix 11.3: Immunohistochemistry

Sodium citrate buffer (pH 6.0) solution

For 1000ml

Tri- sodium citrate (dehydrate).	2.9g
Distilled water	1000ml

Mix to dissolve sodium citrate and adjust pH to 6 with 1ml HCl

Tween 20	0.5ml

Phosphate buffer (pH=7.0) solution

For 2000ml

NaCl	16g
Na_2HPO_4	3.5g
KCl	0.4g
KH_2PO_4	0.4g
Distilled water	2000ml

DAB working solution

DAB chromogen	50µl
Substrate (hydrogen peroxide)	250µl

Primary antibody (Ki-67) dilution factor 1:1200

Phosphate buffer	1200µl
Ki-67	1µl

Remove 1 µl from phosphate buffer and replace with 1200µl of Ki-67 antibody

Methods

Day 1

1. Deparaffinise sections in xylene for 2x 10 minutes
2. Rehydrate sections through graded alcohols
3. Wash slides in running tap water for 5 minutes
4. Antigen retrieve sections in citrate buffer pH 6 (water bath) overnight at 60°

Day 2

5. Allow to cool at room temperature for 20 minutes
6. Wash slides in running tap water for 5 minutes
7. Block endogenous peroxidase with 1% H_2O_2 in methanol for 10 minutes
8. Wash in phosphate buffer solution (PBS) (PH 7.4) for 3x 5 minutes
9. Incubate with normal goat serum 5% (protein block) for 10 minutes
10. Tap serum off slides and wash in PBS for 3x 5 minutes
11. Incubate with primary antibody (Ki-67 1:1200) over night at $4^{o}C$

Day 3

12. Allow sections to reach room temperature for 20 minutes
13. Wash in PBS (pH=7.4) for 3x 5 minutes
14. Incubate with biotinylated secondary antibody 3x 5 minutes
15. Wash in PBS for 3x 5 minutes
16. Incubate with Strep Avidin HRP for 10 minutes
17. Wash in PBS for 3x 5 minutes
18. Incubate with DAB working solution for 5 minutes
19. Rinse in running tap water for 5 minutes
20. Blue with Scott's tap water for 2 minutes
21. Wash in running tap water for 5 minutes
22. Hydrate through graded alcohol
23. Clear in xylene and mount with Entellen

Appendix 12.1 Cell count

1. Import image in to image J (file > open)
2. Go to image on the software and click on image > type > 8 bit
3. Click on process > subtract background and adjust pixel size to 12
4. Click on image > adjust > threshold > apply
5. Click on process > binary > fill holes
6. Click on process > binary > convert to mask
7. Click on process > binary > watershed
8. Click on polygonal selection tool and demarcate region of interest
9. Click on analyse > analyse particles
10. Select bare outline and summarise result on the popped up window
11. Click “OK”

Appendix 12.2: Measurement of cortical thickness

1. Import image (file > open)
2. Select line tool and draw a line along the entire length of the scale bar
3. Select analyse > set scale
4. Type the known distance 2 and the unit of length (mm) in the box that appeared
5. Check on the global and click “OK”
6. Select analyse > tools > ROI manager. A window will appear
7. Select polygonal selection tool
8. Delineate the cross sectional area
9. Click add on the ROI manager
10. Delineate the medullary area
11. Click add on the ROI manager
12. Click measure and calculate the difference

REFERENCES

Abel EL. 1995. An update on incidence of FAS: FAS is not an equal opportunity birth defect. Alcohol Clin Exp Res 17:437-443.

Abel EL, Sokol RJ. 1991. A revised conservative estimate of the incidence of FAS and its economic impact. Alcohol Clin Exp Res 15:514-524.

Barnes DM, Gillett CE. 1995. Determination of cell proliferation. Clin Mol Pathol 48:M2-5.

Bauer JS, Link TM. 2009. Advances in osteoporosis imaging. Eur J Radiol 71:440-449.

Bouxsein ML, Boyd SK, Christiansen BA, Guldberg RE, Jepsen KJ, Müller R. 2010. Guidelines for assessment of bone microstructure in rodents using micro–computed tomography. J Bone Miner Res 25:1468-1486.

Brown D, Gatter K. 1990. Monoclonal antibody Ki-67: its use in histopathology. Histopathology 17:489-503.

Carvan MJ, Loucks E, Weber DN, Williams FE. 2004. Ethanol effects on the developing zebrafish: neurobehavior and skeletal morphogenesis. Neurotoxicol Teratol 26:757-768.

Castania VA, Silveira JWdSd, Issy AC, Pitol DL, Castania ML, Neto AD, Del Bel EA, Defino HLA. 2015. Advantages of a combined method of decalcification compared to EDTA. Microsc Res Tech 78:111-118.

Cederbaum AI. 2012. ALCOHOL METABOLISM. Clinics in liver disease 16:667-685.

Chakkalakal DA. 2005. Alcohol-induced bone loss and deficient bone repair. Alcohol Clin Exp Res 29:2077-2090.

Chakkalakal DA, Novak JR, Fritz ED, Mollner TJ, McVicker DL, Lybarger DL, McGuire MH, Donohue TM, Jr. 2002. Chronic ethanol consumption results in deficient bone repair in rats. Alcohol Alcohol 37:13-20.

Chaudhuri JD. 2000. Alcohol and the developing fetus--a review. Med Sci Monit 6:1031-1041.

Chen H, Hayakawa D, Emura S, Ozawa Y, Taguchi H, Yano R, Shoumura S. 2001. Effects of ethanol on the ultrastructure of the hamster femur. Histol Histopathol 16:763-770.

Chernoff GF. 1977. The fetal alcohol syndrome in mice: an animal model. Teratology 15:223-229.

Clarke B. 2008. Normal bone anatomy and physiology. Clin J Am Soc Nephrol 3 Suppl 3:S131-139.

Conover EA, Jones KL. 2012. Safety concerns regarding binge drinking in pregnancy: A review. Birth Defects Res Part A Clin Mol Teratol 94:570-575.

Control CfD, Prevention. 2003. Fetal alcohol syndrome--South Africa, 2001. MMWR Morb Mortal Wkly Rep 52:660.

Cooper C, Fall C, Egger P, Hobbs R, Eastell R, Barker D. 1997. Growth in infancy and bone mass in later life. Ann Rheum Dis 56:17-21.

Cooper C, Javaid MK, Taylor P, Walker-Bone K, Dennison E, Arden N. 2002. The fetal origins of osteoporotic fracture. Calcif Tissue Int 70:391-394.

Cudd TA. 2005. Animal model systems for the study of alcohol teratology. Bull Exp Biol Med 230:389-393.

D'Elia G, Caracchini G, Cavalli L, Innocenti P. 2009. Bone fragility and imaging techniques. Clin Cases Miner Bone Metab 6:234-246.

Day N, Leech S, Richardson GA, Cornelius M, Robles N, Larkby C. 2002. Prenatal alcohol exposure predicts continued deficits in offspring size at 14 years of age. Alcohol Clin Exp Res 26:1584-1591.

Diamond T, Stiel D, Lunzer M, Wilkinson M, Posen S. 1989. Ethanol reduces bone formation and may cause osteoporosis. Am J Med 86:282-288.

Diez A, Serrano S, Cucurull J, Marinoso L, Bosch J, Puig J, Nogues X, Aubia J. 1997. Acute effects of ethanol on mineral metabolism and trabecular bone in Sprague-Dawley rats. Calcif Tissue Int 61:168-171.

Donnelly E. 2011. Methods for assessing bone quality: a review. Clin Orthop Relat Res 469:2128-2138.

Ducy P, Desbois C, Boyce B, Pinero G, Story B, Dunstan C, Smith E, Bonadio J, Goldstein S, Gundberg C. 1996. Increased bone formation in osteocalcin-deficient mice. Nat 382:448-452.

Duimstra C, Johnson D, Kutsch C, Wang B, Zentner M, Kellerman S, Welty T. 1993. A fetal alcohol syndrome surveillance pilot project in American Indian communities in the Northern Plains. Public health reports (Washington, DC : 1974) 108:225-229.

Ethen MK, Ramadhani TA, Scheuerle AE, Canfield MA, Wyszynski DF, Druschel CM, Romitti PA. 2009. Alcohol consumption by women before and during pregnancy. Matern Child Health J 13:274-285.

Grampp S, Henk CB, Imhof H. 1999. CT and MR assessment of osteoporosis. In: Seminars in Ultrasound, CT and MRI: Elsevier. p 2-9.

Griffith JF, Genant HK. 2011. New imaging modalities in bone. Curr Rheumatol Rep 13:241-250.

Habbick BF, Blakley PM, Houston CS, Snyder RE, Senthilselvan A, Nanson J. 1998. Bone age and growth in fetal alcohol syndrome. Alcohol Clin Exp Res 22:1312-1316.

Hadjidakis DJ, Androulakis, II. 2006. Bone remodeling. Ann N Y Acad Sci 1092:385-396.

Hogan HA, Sampson HW, Cashier E, Ledoux N. 1997. Alcohol consumption by young actively growing rats: a study of cortical bone histomorphometry and mechanical properties. Alcohol Clin Exp Res 21:809-816.

Hoyme HE, May PA, Kalberg WO, Kodituwakku P, Gossage JP, Trujillo PM, Buckley DG, Miller JH, Aragon AS, Khaole N. 2005. A practical clinical approach to diagnosis of fetal alcohol spectrum disorders: clarification of the 1996 institute of medicine criteria. Pediatrics 115:39-47.

Johnell O, Kanis J. 2006. An estimate of the worldwide prevalence and disability associated with osteoporotic fractures. Osteoporos Int 17:1726-1733.

Jones G, Dwyer T. 2000. Birth weight, birth length, and bone density in prepubertal children: evidence for an association that may be mediated by genetic factors. Calcif Tissue Int 67:304-308.

Jones K, Smith D. 1973. Recognition of the fetal alcohol syndrome in early infancy. The Lancet 302:999-1001.

Junqueira LC, Carneiro J. 2005. Basic histology text and atlas: London: McGraw Hill, 2005.

Keiver K, Herbert L, Weinberg J. 1996. Effect of maternal ethanol consumption on maternal and fetal calcium metabolism. Alcohol Clin Exp Res 20:1305-1312.

Keiver K, Weinberg J. 2004. Effect of duration of maternal alcohol consumption on calcium metabolism and bone in the fetal rat. Alcohol Clin Exp Res 28:456-467.

Kherlopian AR, Song T, Duan Q, Neimark MA, Po MJ, Gohagan JK, Laine AF. 2008. A review of imaging techniques for systems biology. BMC Syst Biol 2:74.

Kierszenbaum AL, Tres L. 2015. Histology and Cell Biology: An Introduction to Pathology E-Book: Elsevier Health Sciences.

Kramer B, Allan J. 2005. Fundamentals of Human Osteology: Lexisnexis Butterworths.

Landgraf MN, Nothacker M, Kopp IB, Heinen F. 2013. The diagnosis of fetal alcohol syndrome. Dtsch Arztebl Int 110:703.

Link TM, Majumdar S. 2004. Current diagnostic techniques in the evaluation of bone architecture. Curr Osteoporos Rep 2:47-52.

Lui JC, Nilsson O, Baron J. 2011. Growth plate senescence and catch-up growth. Endocrine development 21:23-29.

Maddalozzo GF, Turner RT, Edwards CH, Howe KS, Widrick JJ, Rosen CJ, Iwaniec UT. 2009. Alcohol alters whole body composition, inhibits bone formation, and increases bone marrow adiposity in rats. Osteoporos Int 20:1529-1538.

Marcus R, Feldman D, Nelson D, Rosen CJ. 2009. Fundamentals of osteoporosis: Academic Press.

Maurel D. B, Boisseau N, Benhamou C. L, Jaffre C. 2012. Alcohol and bone: review of dose effects and mechanisms. Curr Osteoporos Rep 23:1-16.

May PA, Brooke L, Gossage JP, Croxford J, Adnams C, Jones KL, Robinson L, Viljoen D. 2000. Epidemiology of fetal alcohol syndrome in a South African community in the Western Cape Province. Am J Public Health 90:1905.

May PA, Fiorentino D, Phillip Gossage J, Kalberg WO, Eugene Hoyme H, Robinson LK, Coriale G, Jones KL, Del Campo M, Tarani L. 2006. Epidemiology of FASD in a province in Italy: prevalence and characteristics of children in a random sample of schools. Alcohol Clin Exp Res 30:1562-1575.

May PA, Gossage JP, Marais A-S, Adnams CM, Hoyme HE, Jones KL, Robinson LK, Khaole NC, Snell C, Kalberg WO. 2007. The epidemiology of fetal alcohol syndrome and partial FAS in a South African community. Drug Alcohol Depend 88:259-271.

May PA, Marais A-S, Gossage JP, Barnard R, Joubert B, Cloete M, Hendricks N, Roux S, Blom A, Steenekamp J, Alexander T, Andreas R, Human S, Snell C, Seedat S, Parry CC, Kalberg WO, Buckley D, Blankenship J. 2013. Case management reduces drinking during pregnancy among high risk women. Int J Alcohol Drug Res 2:61-70.

McCall T, Fassett D, Brockmeyer B. 2006. Cervical spine trauma in children: a review. Neurosurg Focus 20:1-8.

Mehta G, Roach H, Langley-Evans S, Taylor P, Reading I, Oreffo R, Aihie-Sayer A, Clarke N, Cooper C. 2002. Intrauterine exposure to a maternal low protein diet reduces adult bone mass and alters growth plate morphology in rats. Calcif Tissue Int 71:493-498.

Memo L, Gnoato E, Caminiti S, Pichini S, Tarani L. 2013. Fetal alcohol spectrum disorders and fetal alcohol syndrome: the state of the art and new diagnostic tools. Early Hum Dev 89:S40-S43.

Mikosch P. 2014. Alcohol and bone. Wien Med Wochenschr 164:15-24.

Miralles-Flores C, Delgado-Baeza E. 1992. Histomorphometric analysis of the epiphyseal growth plate in rats after prenatal alcohol exposure. J Orthop Res 10:325-336.

Mishra S, Sahai A, Srivastava A, Agrawal A, Singh P, Mishra R. 2003. Skeletal anomalies in fetal alcohol syndrome: a study on developing mice embryos. J Anat Soc India 52:51-54.

Nilsson O, Baron J. 2004. Fundamental limits on longitudinal bone growth: growth plate senescence and epiphyseal fusion. Trends Endocrinol Metab 15:370-374.

Nwaogu IC. 2002. Growth rate of bones in rat foetal alcohol syndrome. Vet Arh 72:343-351.

O'Leary CM. 2004. Fetal alcohol syndrome: diagnosis, epidemiology, and developmental outcomes. J Paediatr Child Health 40:2-7.

Parry CD. 2005. South Africa: alcohol today. Addiction 100:426-429.

Patten AR, Fontaine CJ, Christie BR. 2014. A comparison of the different animal models of fetal alcohol spectrum disorders and their use in studying complex behaviors. Front Pediatr 2:19.

Peltzer K, Davids A, Njuho P. 2011. Alcohol use and problem drinking in South Africa: findings from a national population-based survey. Afr J Psychiatry 14:7.

Percival CJ, Richtsmeier JT. 2013. Angiogenesis and intramembranous osteogenesis. Dev Dynam 242:909-922.

Ramadoss J, Hogan HA, Given JC, West JR, Cudd TA. 2006. Binge alcohol exposure during all three trimesters alters bone strength and growth in fetal sheep. Alcohol 38:185-192.

Ramos-Vara J. 2005. Technical aspects of immunohistochemistry. Vet Pathol 42:405-426.

Reece JB, Urry LA, Cain ML, Wasserman SA, Minorsky PV, Jackson R. 2014. Campbell biology: Pearson Boston.

Reed AH, McCarty HL, Evans GL, Turner RT, Westerlind KC. 2002. The effects of chronic alcohol consumption and exercise on the skeleton of adult male rats. Alcohol Clin Exp Res 26:1269-1274.

Refinetti R. 1989. Body size and metabolic rate in the laboratory rat. Exp Biol 48:291-294.

Sampson HW, Chaffin C, Lange J, DeFee B, 2nd. 1997a. Alcohol consumption by young actively growing rats: a histomorphometric study of cancellous bone. Alcohol Clin Exp Res 21:352-359.

Sampson HW, Perks N, Champney TH, DeFee B, 2nd. 1996. Alcohol consumption inhibits bone growth and development in young actively growing rats. Alcohol Clin Exp Res 20:1375-1384.

Sampson PD, Streissguth AP, Bookstein FL, Little RE, Clarren SK, Dehaene P, Hanson JW, Graham JM. 1997b. Incidence of fetal alcohol syndrome and prevalence of alcohol-related neurodevelopmental disorder. Teratology 56:317-326.

Schneider M, Norman R, Parry C, Bradshaw D, Pluddemann A, Collaboration SACRA. 2007. Estimating the burden of disease attributable to alcohol use in South Africa in 2000. S Afr Med J 97:664-672.

Scholzen T, Gerdes J. 2000. The Ki-67 protein: from the known and the unknown. J Cell Physiol 182:311-322.

Shi S-R, Cote RJ, Taylor CR. 2001. Antigen retrieval techniques: current perspectives. J Histochem Cytochem 49:931-937.

Simpson ME, Duggal S, Keiver K. 2005. Prenatal ethanol exposure has differential effects on fetal growth and skeletal ossification. Bone 36:521-532.

Slade T, Chapman C, Swift W, Keyes K, Tonks Z, Teesson M. 2016. Birth cohort trends in the global epidemiology of alcohol use and alcohol-related harms in men and women: systematic review and metaregression. BMJ open 6:e011827.

Smith DF, Sandor GG, MacLeod PM, Tredwell S, Wood B, Newman DE. 1981. Intrinsic defects in the fetal alcohol syndrome: studies on 76 cases from British Columbia and the Yukon Territory. Neurotoxicol. Teratol. 3:145-152.

Snow M, Keiver K. 2007. Prenatal ethanol exposure disrupts the histological stages of fetal bone development. Bone 41:181-187.

Soares EV, Fávaro WJ, Cagnon VH, Bertran CA, Camilli JA. 2010. Effects of alcohol and nicotine on the mechanical resistance of bone and bone neoformation around hydroxyapatite implants. J Bone Miner Metab 28:101.

Sokol RJ, Clarren SK. 1989. Guidelines for use of terminology describing the impact of prenatal alcohol on the offspring. Alcohol Clin Exp Res 13:597-598.

Sokol RJ, Delaney-Black V, Nordstrom B. 2003. Fetal alcohol spectrum disorder. JAMA 290:2996-2999.

Spohr HL, Willms J, Steinhausen HC. 1993. Prenatal alcohol exposure and long-term developmental consequences. Lancet (London, England) 341:907-910.

Streissguth AP, Aase JM, Clarren SK, Randels SP, LaDue RA, Smith DF. 1991. Fetal alcohol syndrome in adolescents and adults. JAMA 265:1961-1967.

Turner R, Doran E, T. Iwaniec U. 2012. Detrimental Effects of Alcohol on Bone Growth.

Turner RT, Kidder LS, Kennedy A, Evans GL, Sibonga JD. 2001. Moderate alcohol consumption suppresses bone turnover in adult female rats. J Bone Miner Res 16:589-594.

Urban M, Chersich MF, Fourie L-A, Chetty C, Olivier L, Viljoen D. 2008. Fetal alcohol syndrome among grade 1 schoolchildren in Northern Cape Province: prevalence and risk factors. S Afr Med J 98:877-882.

Viljoen DL, Gossage JP, Brooke L, Adnams CM, Jones KL, Robinson LK, Hoyme HE, Snell C, Khaole NC, Kodituwakku P. 2005. Fetal alcohol syndrome epidemiology in a South African community: a second study of a very high prevalence area. J Stud Alcohol 66:593-604.

Warren KR, Calhoun FJ, May PA, Viljoen DL, Li TK, Tanaka H, Marinicheva GS, Robinson LK, Mundle G. 2001. Fetal alcohol syndrome: an international perspective. Alcohol Clin Exp Res 25: 202S-206S.

Weiner S, Traub W, Wagner HD. 1999. Lamellar bone: structure–function relations. J Struct Biol 126:241-255.

Wezeman FH, Emanuele MA, Emanuele NV, Moskal SF, 2nd, Woods M, Suri M, Steiner J, LaPaglia N. 1999. Chronic alcohol consumption during male rat adolescence impairs skeletal development through effects on osteoblast gene expression, bone mineral density, and bone strength. Alcohol Clin Exp Res 23:1534-1542.

White A, Castle IJP, Chen CM, Shirley M, Roach D, Hingson R. 2015. Converging patterns of alcohol use and related outcomes among females and males in the United States, 2002 to 2012. Alcohol Clin Exp Res 39:1712-1726.

White TD, Black MT, Folkens PA. 2011. Human osteology: Academic press.

Wilsnack RW, Wilsnack SC, Kristjanson AF, Vogeltanz-Holm ND, Gmel G. 2009. Gender and alcohol consumption: patterns from the multinational GENACIS project. Addiction 104:1487-1500.

Young B, Woodford P, O'Dowd G. 2013. Wheater's Functional Histology E-Book: A Text and Colour Atlas: Elsevier Health Sciences.